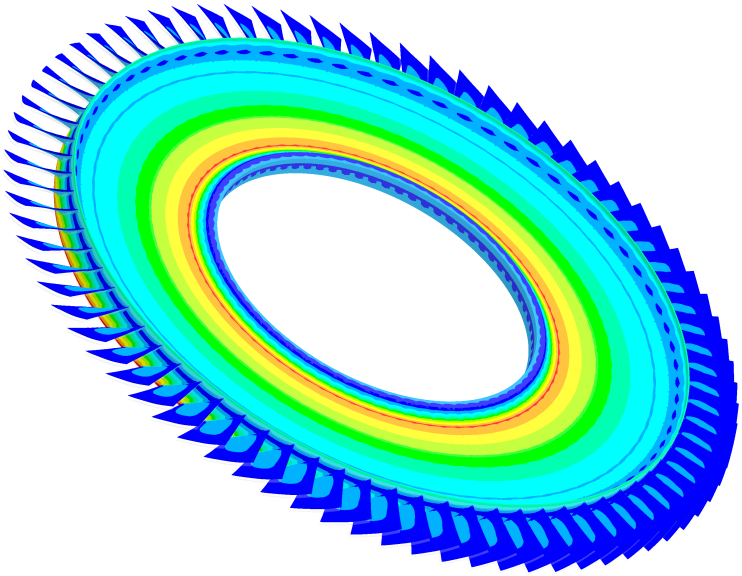

Research and Development of Additive Manufactured Bladed Disks

Collaboration between Chalmers, Penn State and GKN Aerospace

Bachelor's thesis in Mechanical Engineering

John Austin Bayliff
Adam Billberg
Rasmus Blom
Nicole Gallegor
Oscar Holke
Stephen Sandford

Department of Applied Mechanics

CHALMERS UNIVERSITY OF TECHNOLOGY
Gothenburg, Sweden 2017

Department of Mechanical and Nuclear Engineering
PENNSYLVANIA STATE UNIVERSITY
State College, Pennsylvania, United States of America 2017

Bachelor's thesis 2017:09

Research and Development of Additive Manufactured Bladed Disks

Collaboration between Chalmers, Penn State and GKN Aerospace

John Austin Bayliff
Adam Billberg
Rasmus Blom
Nicole Gallegor
Oscar Holke
Stephen Sandford

Department of Applied Mechanics
Chalmers University of Technology
Gothenburg, Sweden 2017
Department of Mechanical and Nuclear Engineering
Pennsylvania State University
State College, Pennsylvania, The United States of America, 2017

Research and Development of Additive Manufactured Bladed Disks
Collaboration between Chalmers, Penn State and GKN Aerospace
JOHN AUSTIN BAYLIFF, ADAM BILLBERG, RASMUS BLOM, NICOLE GALLEGOR, OSCAR HOLKE, STEPHEN SANDFORD

Supervisor: Prof. Mikael Enelund, Department of Applied Mechanics
Examinor: Prof. Magnus Ekh, Department of Applied Mechanics
Supervisor: Prof. Jason Moore, Department of Mechanical and Nuclear Engineering

Bachelor's Thesis 2017:09
ISSN 1654-4676 Department of Applied Mechanics
Chalmers University of Technology
SE-412 96 Gothenburg
Telephone +46 31 772 1000

Printed by Chalmers Reproservice
Chalmers University of Technology
Gothenburg, Sweden 2017

Research and Development of Additive Manufactured Bladed Disks
Collaboration between Chalmers, Penn State and GKN Aerospace
J. BAYLIFF, A. BILLBERG, R. BLOM, N. GALLEGOR, O. HOLKE, S. SANDFORD

Abstract

The contemporary manufacturing methods for bladed disks, also known as "blisks", cause a great deal of material waste. To reduce the material waste and increase the freedom of design, GKN Aerospace requested this project to evaluate additive manufacturing (AM) as a manufacturing method for blisks. Additive manufacturing methods were researched and evaluated based on mechanical properties, freedom of design, material use, and production times. Finite Element Analyses with respective rotation and pressures have been performed and reviewed. All researched methods have been found to have the ability to fulfill the requirements by GKN Aerospace: Power Bed Fusion (PBF) methods and Direct Energy Deposition (DED) methods.

This bachelor thesis is a collaboration between GKN Aerospace and students from Chalmers University of Technology and Pennsylvania State University. GKN Aerospace provided the project with CAD models on the current blisk design as well as data about loads and temperatures for the simulations. They also provided a list of parameters for the design including restrictive safety standards and production times. GKN Aerospace stated that Titanium-64 ($TiAl_6V_4$) is the preferred metal alloy for production. A large part of the project was to examine and study different methods of additive manufacturing in consideration for the production of blisks. The best method was identified and specified to fit the needs of GKN Aerospace. The team had access to a running Gantt Chart scheduling tool to remain on task and ensure that all parameters of the project were met throughout the semester long project. The team also stayed within the outlined budget, only spending $260.56 on travel and prototyping expenses.

The main problem with contemporary additive manufacturing machines utilizing PBF are their relatively small size which led to researching joining techniques. For the DED methods researched, the main problem faced were geometric restrictions in printing complex structures. After reviewing the objectives and comparing them using a Pugh matrix, it was determined what concept would work best for GKN Aerospace. Electron Beam Melting (EBM), a PFB method, should first be used to print the blisk in sections. Then, the pieces should be joined together using Electron Beam Welding (EBW). After this the blisk should be heat treated using HIP and finally machined to reach desirable surface textures. Further evaluation of the mechanical properties of EBM $TiAl_6V_4$ and EBW will need to be done by GKN Aerospace to ensure this design will work for this particular aerospace application should they choose to move forward with this concept.

Keywords: Additive Manufacturing, $TiAl_6V_4$, bladed disk, blisk, EBM, EBW

Sammandrag

Den nutida tillverkningsmetoden för bladed disks, även kallade "blisks", orsakar stora materialförluster. För att minska på materialförlusterna och öka designfriheten har GKN Aerospace försett projektet med uppgiften att utvärdera additiv tillverkning (AM) som en tillverkningsmetod för blisks. Metoder för additiv tillverkning undersöktes och utvärderades med avseende på mekaniska egenskaper, designfrihet, materialanvändning, och produktionstider. Finita element analyser genomfördes med tryck och rotation implementerat vilka sedan analyserades. Projektet kom fram till att alla studerade AM metoder klarar de krav som ställts av GKN Aerospace: Powder Bed Fusion (PBF) metoder och Direct Energy Deposition (DED) metoder.

Denna kandidatuppsatts är ett samarbete mellan GKN Aerospace, studenter från Chalmers tekniska högskola samt studenter från Pennsylvania State University. GKN Aerospace tillhandahåll projektet med CAD modeller av en blisk samt data om laster och temperaturer för simuleringarna. De tillhandahöll även en lista över parametrar för designen såsom säkerhetsparametrar och produktionsparametrar. GKN Aerospace angav att det är önskvärt att använda legeringen ($TiAl_6V_4$) för produktionen. En stor del av projektet har bestått av att undersöka AM metoder som kan tillämpas i projektet. Den bästa metoden identifierades och specificerades för att passa GKN Aerospaces behov. Laget hade tillgång till ett löpande Ganttschema för att inte avvika från uppgiften och se till att projektets tid användes väl. Laget höll sig även inom den angivna budgeten och använde endast 2300 kr för resor och prototypkostnader.

Det största problemet med AM maskiner som nyttjar PBF är deras relativt små utskriftskammare vilket ledde till att även fogningsmetoder undersöktes. För DED var det största problemet restriktioner i att skriva ut komplicerade geometrier. Efter att ha utvärderat målen i projektet valdes det bästa konceptet, som uppfyllde GKN Aerospaces mål bäst, ut genom att använda en Pughmatris. Electron Beam Melting (EBM) som är en metod för PBF, ska först användas för att skriva ut blisken i sektioner. Dessa delar ska sedan fogas samman med Electron Beam Welding (EBM). Efter detta ska delarna värmebehandlas med HIP och slutligen svarvas så att en tillräckligt fin yta uppnås. Ytterligare utvärdering av materialegenskaperna för $TiAl_6V_4$ och egenskaper hos EBW bör genomföras av GKN Aerospace om de väljer att vidareutveckla konceptet.

Nyckelord: Additiv tillverkning, $TiAl_6V_4$, bladed disk, blisk, 3D-skrivning, EBM, EBW

Acknowledgements

The group has had help from several external sources, and we would like to thank them for their contributions to this report. At Penn State, professors Tim Simpson and Todd Palmer provided feedback on concepts based on their expertise in additive manufacturing. A special thanks is given to Mikael Enelund and Jason Moore for working closely with the team throughout the course of the project. A big thanks to the Mechanical Engineering department at Chalmers and (again) Mikael Enelund, for sponsoring and administrating the visit to Penn State for the Chalmers students. It was very appreciated!

Additionally, the group thank GKN Aerospace for providing a challenging and rewarding project and Stefan Forsman for offering guidance and feedback throughout the project.

R. Blom, A. Billberg, O. Holke, Gothenburg, 2017
J. Bayliff, N. Gallegor, S. Sandford, State College Pennsylvania, 2017

Nomenclature

The next list describes several abbreviations and symbols that will later be used within the body of the document.

Additive manufacturing methods

AM	Additive Manufacturing
DED	Direct Energy Deposition
DMLM	Direct Metal Laser Melting
DMLS	Direct Metal Laser Sintering
EBAM	Electron Beam Additive Manufacturing
EBM	Electron Beam Melting
LENS	Laser Engineering Net System
PBF	Powder Bed Fusion
SLM	Selective Laser Melting
SLS	Selective Laser Sintering

Other

AHP	Analytic Hierarchy Process
ASME	American Society of Mechanical Engineers
ASTM	American Society for Testing and Materials International
CAD	Computer Aided Design
CNC	Computer Numerical Control
PLA	Polylactic acid
UTS	Ultimate Tensile Strength

Post processing

CIP	Cold isostatic pressing
HIP	Hot isostatic pressing

List of symbols

α	Angle of blade between axial and tangential direction
ω	Rotational velocity
A_{tot}	Combined front surface area of all blades
F_{normal}	Force normal to blade
F_{tan}	Force tangential to blisk rim
M	Moment
P	Work
p	Pressure on blade
r	Radius to centre of blade

Welding methods

EBW	Electron Beam Welding

GTAW	Gas Tungsten Arc Welding
LFW	Linear Friction Welding

Contents

List of Figures

List of Tables

1
Introduction

The production of aerospace bladed fan disks is restricted by current forging and manufacturing processes. Machining parts can often lead to warping of the finished product or chipping. The functionality and compatibility of the finished bladed disk can decrease as the parts are mismanufactured. Additive manufacturing (AM) has allowed for more freedom in the design of complex systems to be safer, more aerodynamic, and more customized. These methods also create one solid part rather than having multiple assembly steps as in current dovetail designs. A variety of AM methods are at the disposal of the aerospace industry including, but not restricted to, Electron Beam Melting (EBM), Direct Metal Laser Sintering (DMLS), Directed Energy Deposition (DED), and Selective Laser Melting (SLM). Each method offers its own set of benefits as well as drawbacks.

1.1 Initial Problem Statement

Bladed disks, often referred to as blisks, are becoming more common in jet engines. Blisks can offer improved performance, larger design freedom, and are lighter than conventional disks, however, because blisks are machined from a single piece of metal, there is substantial material waste. This makes repairing and replacing blisks quite expensive. To overcome these material losses, AM methods are being researched as a future manufacturing method for blisks. Aside from improving reliability, multiple safety factors will also need to be considered when working with a rotating part such as a blisk.

This semester, in a joint effort, students at Chalmers and Penn State worked together to research the AM capabilities for blisks. GKN Aerospace served as the industrial partner and provided information to the students assisting them throughout the course of the project. GKN Aerospace is a well respected company in their industry with a large interest in advanced manufacturing technologies. The team was able to provide GKN with a feasible manufacturing design and recommendations of how to produce a blisk utilizing AM.

1.2 Objectives

The goal of the project was to design a blisk that, with the use of AM, lowers the material use significantly while maintaining the high performance of machined disks. The blisk also needed to be able to be withstand at least 30,000 start-stop

cycles. Two existing AM methods were explored to determine the best option for GKN: Powder Bed Fusion (PBF) and Direct Energy Deposition (DED). The final project also consisted of the specification of the requirements for the AM method to ensure that the produced blisks are competitive alternatives. In addition to selecting a suitable AM method for GKN, a second goal included providing a structural analysis of the blisk design. Throughout the project, there were several limitations and assumptions necessary to create a final proposal including the building envelope size, limited economic data, and weakness of reputable material data.

1.2.1 Scope of Work

The project began with the identification of key performance indicators for blisks to ensure that the blisks manufactured through AM would meet the performance requirements. Furthermore, a literature survey on AM-methods was carried out and a final method was chosen that is believed to ensure the best result. The AM-methods were evaluated with respect to the performance of the part.

The current blisk design was evaluated using computer simulations with ANSYS software [6] during operational conditions focusing on stresses and the fatigue life. With this information the capabilities of AM methods for the parts were identified. The entire blisk could not be manufactured through AM in its entirety; therefore, a separate joining and production method was investigated for the interfaces between manufactured parts and AM parts.

1.2.2 Limitations

The project was restricted by a time constraint that played a factor in the final results of the project. The project team composed of three students from Chalmers and three student from PSU. The students from Chalmers worked on the project from January 17th to May 23rd and the students from PSU worked on the project from January 9th to May 1st.

Because of the students' limited knowledge in this area of expertise, this lead to further limitations on the project. However, all students had some earlier experience and knowledge in the areas. The project utilized the supervisors' and other external parties knowledge in areas like material properties, simulations and manufacturing techniques to make sure that correct assessments were made.

Due to restrictions in budget, the team was unable to manufacture the final design as a metal prototype. Instead, a single blade was printed in aluminum from an external company to use as a demonstration of the rough surface finish associated with AM methods. A geometrically similar plastic prototype and analysis of the final design in metal were also done to support the recommendations being made. Furthermore, no physical tests on the AM-method were performed. Instead the sole focus of the project was on theoretical analysis and computer simulations of the design.

Safety factors had to remain within the same ranges as the current production methods. Tolerances of the dimensions and the restrictions of the blisk environment also had to comply with the current blisk designs and methods. Ultimately, the final design for the AM blisks had to fit the current assembly to be useful for GKN Aerospace.

Due to the low level of maturity in the area of metal AM, a distinctive lack of data made limitations on possible areas of evaluation necessary. One of these was the evaluation of creep properties.

AM enable exotic designs in the center parts of the blisk (disk) as well as in the blades. It can enable weight reductions by creating hollow and web-like structures. This is one of the reasons to why the group has chosen to limit the project to only include blisks made using only AM methods. No combination of AM and conventional production methods will be evaluated more than briefly. A limitation was also made to only evaluate solid blisks.

2
Theory

Since the subject of AM is relatively new, there is for many studies a lack of information. The information that exists must be critically reviewed. That is why a comprehensive external search has been conducted, especially regarding material properties from different AM methods, and what characterizes them.

2.1 Existing Rotors

There are two main types of rotors used in the compressor part of today's turbofan jet engines: conventional rotors and bladed disks. The main difference between them is that conventional rotors have removable blades while bladed disks are machined from a single piece of metal. [2, 1]

2.1.1 Conventional Compressor Rotors

The center part of the rotor will from now on be called the "disk". The "blades" are the thin parts fastened on the outer rim of the disk. For conventional compressor rotors the disk and blades are manufactured separately and then joined together [25]. The disks are manufactured by either powder metallurgy, or machine cutting and stamping, while machining is used to form the the blades. Dovetail joints are frequently used to attach the blades to the disk [9]. Conventional rotors benefit from being able to exchange single blades if they would become damaged.

2.1.2 Bladed Disks

Bladed disks, or blisks, are the name of disks with the blades directly attached to the center disk. This is achieved by milling the entire blisk from one solid block of metal, rather than creating the blades separately and then assembling it. The benefits of this are an increase in fuel efficiency by up to 8% [13] and a reduced risk of crack initiation [55]. However, a disadvantage with blisks is that there is no easy way of repairing a damaged one. They also have to go through rigorous harmonic vibration testing and dynamic balancing, because the natural damping provided by a dovetail attachment is no longer present [55].

2.2 Patents

In the external search process in the beginning of the project a patent search was conducted. This was due to the unknown complexity and maturity of the area of expertise, AM of complex high performance blisks. If the search found a comprehensive number of patents within the area it would be a sign of higher maturity. The patents themselves could then be used to make an early assessment of the complexity of the task to create a blisk using AM.

The external search for existing patents was done using Espacenet as well as Google's Patent database. Two patents were found that relate to the project as well as the final product itself. Full descriptions of the two patents can be found in Appendix C. The first of these is Patent US2009283503 owned by Rolls Royce Deutschland Ltd & Co KG, Germany. In short the patent is about utilizing laser brazing to form a blisk by joining the disk and the blades with a nickel or titanium-base material. The second patent is US2016348517 owned by General Electric. This patent regards to utilizing AM to form internal cooling in a blisk.

The low number of patents found indicates a low maturity of the area which is strengthened by the fact that no other blisk manufacturer that was researched was found to currently manufacture blisks utilizing AM. From the relative low complexity of the patents it can be said that the task itself should be relatively hard since the patents otherwise would not have been approved.

2.3 Additive Manufacturing methods

Today large varieties of metal AM methods exist. They all produce materials with different properties and they all also have their own benefits and drawbacks. Some do not need support structures, some are very quick, and some have high precision.

2.3.1 Powder Bed Fusion

The three main techniques regarding PBF are DMLS, SLM and EBM. PBF works by melting a metal powder, that has been spread out by a roller, by either a laser or an electron beam. The subsequent layer is spread out across the previous layer, and the process is repeated. The powder is spread out by either a roller or a recoater blade [4]. There are numerous examples exhibiting the use of DMLS and SLM throughout the aerospace industry. Some examples include Airbus Defense and Space's Titanium Satellite clamps and GE Aviation's Engine Fuel Nozzle [52]. PBF methods provide several key advantages such as their geometric complexity benefits as well as near full density (99.5+%) when compared to conventionally manufactured parts [29], for illustration see Figure 2.1.

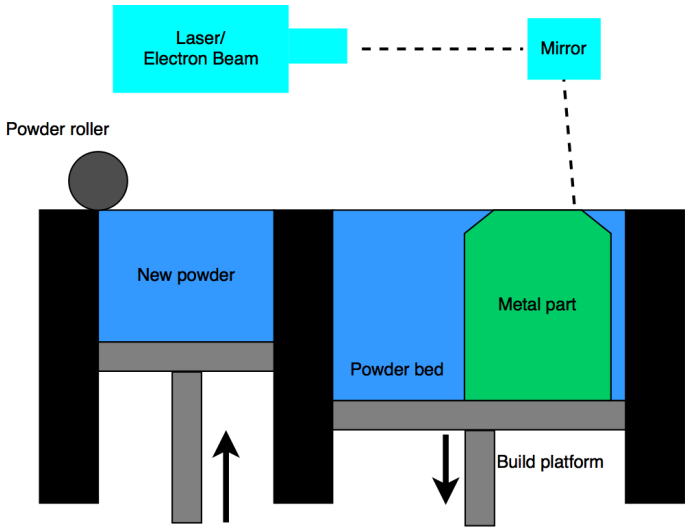

Figure 2.1: Illustration of Powder Bed Fusion method with powder roller.

2.3.1.1 Direct Metal Laser Sintering

The DMLS, sometimes called SLS, process takes place in an enclosed chamber filled with nitrogen or argon gas. A laser beam is then used to thermally fuse the powder together, at the desired places. The surrounding powder that is not melted serves as support structures [22, 7]. Since the powder is not melted but sintered, DMLS enables the process to include multiple different alloys at once [28].

2.3.1.2 Selective Laser Melting

SLM works similarly to DMLS with a powder that is spread out and a laser that joins the powder together. The difference is that SLM melts the material completely, resulting in higher density. However, this also means that the SLM process generally requires more energy since the material needs to be heated above its melting point. Furthermore, the solidification after melting can also induce residual stresses in the material [3].

2.3.1.3 Electron Beam Melting

EBM is very similar to SLM with the main difference being that EBM uses an electron beam instead of a laser to melt the powder. EBM also uses a vacuum chamber instead of a protective gas and has a high build temperature of around 700 °C. The EBM method benefits from being more efficient than laser systems since much of the energy of the laser is lost as it is reflected, instead of being absorbed, by the powder as well has not having any residual stresses due to the high build temperature [22].

2.3.2 Direct Energy Deposition

DED, also known as Direct Metal Deposition (DMD), is an AM method that uses a metal wire or powder that is fed out of feed nozzles and melted, by either laser or

electron beam, as it is deposited on the part [22]. The feed nozzle moves in three dimensions across the part and melts a line of material with every pass, building a 3D geometry. Because DED deposits the material it is possible to vary the material during the process. It is also possible to closely control the micro structure by changing process parameters. However, DED is limited in terms of producing complex structures as it needs dense support structures. In addition, DED suffer from poor surface finish with Ra values below 25 μm being hard to achieve. The DED process is illustrated in Figure 2.2

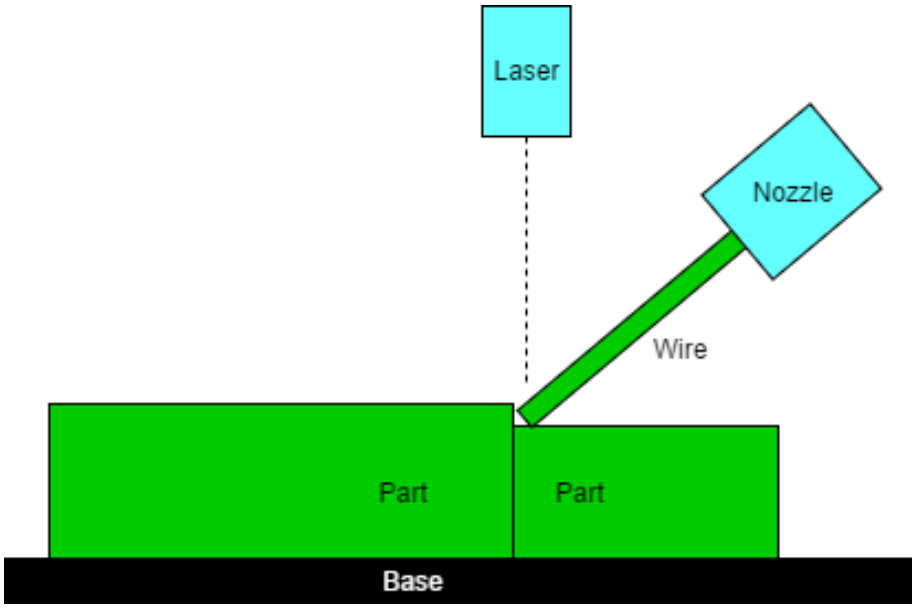

Figure 2.2: Example of DED process

2.4 Additive Manufacturing Machines

A study of today's machines for AM yields that, depending on printing method, the maximum print size varies widely. Below some examples of 3D-printers are presented that are able to print in $TiAl_6V_4$, but utilize different AM methods. The examples are also chosen to show the maximum printing dimensions of the different methods.

Sciaky's [42] EBAM™ 300 System utilizes Electron Beam Additive Manufacturing (EBAM) a type of DED which has the maximum printing dimensions 5791 x 1219 x 1219 mm^3 [43]. During an interview with representatives of Arcam AB, they spoke about their Arcam A2X system which utilizes EBM and has maximum working dimensions of 200 x 200 x 380 mm^3 [1]. According to the representatives interviewed, these dimensions are in the upper level within the area of AM methods for PBF systems. EOS e-manufacturing solutions [17], one of Arcam AB's main competitors,

[1]Representatives Arcam AB. 2017. Interview February 8 at Chalmers University of Technology during a meeting with 4 engineers from the company that was there to promote Arcam AB as an employer.

has a similar printer, the EOS M 290. This printer utilizes SLS rather than EBM and is able to print in dimensions 250 x 250 x 325 mm^3 [50]. These dimensions are in line with the comment from Arcam AB that their system is in the larger dimensions for PDF AM today.

2.5 Print Speeds of Additive Manufacturing Methods

In determining build speed using AM methods, there are multiple factors to consider. The numerous manufacturers and machines have different build speeds for different reasons. Factors to consider, depending on the AM method chosen, include: nozzle temperature, material, layer thickness, number of supports required, desired quality, and laser power among others. For this reason, it can be difficult to calculate an exact production time. In Table 2.1 build speeds for several AM methods are presented.

Table 2.1: Production Speed from Ek's Thesis [20]

Method	Machine supplier	Build Speed	Material
EBM	Arcam	266 g/h	$TiAl_6V_4$
DMLS	EOS	60-143 g/h	$TiAl_6V_4$
SLM	MCP Realizer	3-4.5 g/h	$TiAl_6V_4$
DED	LENS 850R (Optomec)	500 g/h	Not specified

2.6 Properties of Additive Manufactured $TiAl_6V_4$

Through an extensive literature survey properties of additive manufactured $TiAl_6V_4$ have been compiled. A general theme throughout the survey is the uncertainty of data where consistent reliable data is infrequent. The data presented in this section is not the minimum values but rather average data that correspond well to the application. Minimum values could not be used as the research presenting these values are not consistent and often do not use correct process parameters.

2.6.1 Mechanical Properties of Additive Manufactured $TiAl_6V_4$

The tensile properties of PBF printed $TiAl_6V_4$ will differ depending on the processes that have been used. This is because of different temperatures and cooling rates which changes the micro structure of the material. Parts produced by SLM will, because of their martensite structure, have higher yield strengths but lower ductility compared to parts produced by EBM, with $\alpha + \beta$ structure [31]. The as-built SLM and DMLS material will, because of the high cooling rate, have some residual stresses. This can be overcome with stress relieving by heat treatments to increase the ductility. For example, transforming the martensite into $\alpha + \beta$ phase will increase the ductility [44, 8].

For tensile properties for powder DED $TiAl_6V_4$, Wu *et al.* [53] found that the micro structure depend on the laser power and the powder feed rate. With low laser power pores form in the sample. The porosity increases with decreased laser power. At and above roughly 260 W the pores are no longer present. The micro structure is mainly lamellar with $\alpha+\beta$ laths that increase in size with increased laser power and feed rate. Qiu *et al.* [38] describe the structure as dominated by columnar grains and martensitic needle structure. After heat treatment by HIP the martensite was transformed into lamellar $\alpha + \beta$. The values for as-built DED are similar to the values reported by Wu *et al.*, however, with a decrease in ultimate tensile strength. The heat treatment lowered the yield and ultimate tensile strengths but increased the ductility.

Data for Tensile and ultimate yield strengths for as-built EBM, as-built SLM, heat treated SLM, as-built DMLS, as-built powder DED, and HIP powder DED for $TiAl_6V_4$ are found in Table 2.2.

Table 2.2: Tensile and ultimate yield strength for a variety of AM methods with $TiAl_6V_4$.

Process	Tensile Yield Strength (MPa)	Ultimate Yield Strength (MPa)	Reference
EBM as-built (XY)	975	1023.5	[40]
EBM as built (Z)	972	1021	[40]
SLM as-built (XY)	1060	1230	[31]
SLM as-built (Z)	1070	1200	[44]
SLM heat treated (XY)	955	1004	[51]
DMLS as-built	967	1131	[8]
DED powder as-built (XY)	960	1063	[12]
DED powder as-built (Z)	970	1087	[12]
DED HIPed	850	920	[38]

With tests according to ASTM E 8 standards [46], Rawal *et al.* determined the elastic modulus of EBM manufactured $TiAl_6V_4$ [39]. Their tests also determined yield strength and ultimate strengths receiving similar values as previously stated. They also showed that the elastic modulus at room temperature was slightly higher than the one at 121° C. For SLM, with tests according to ASTM E 111 [45], the elastic modulus, in the xy-direction, which is the horizontal plane in the machine, was determined by Vrancken *et al.* [51]. Their tests were done on both as-built and heat treated SLM and the results were in accordance to what was stated earlier. The heat treatment, except for water quenching, increased the ductility and decreased the yield and tensile strengths. Tests on as-built SLS were done on samples according to ASTM E 8M [8]. For DED with powder, Sterling *et al.* [47] determined the elastic modulus, with test in accordance to ASTM E 8M [46]. The results from all tests are shown in Table 2.3. Note that the spread in elastic moduli is small.

Table 2.3: Elastic modulus for a variety of AM methods with $TiAl_6V_4$.

Process	Elastic modulus (GPa)	Reference
EBM Mean (XY)	114.4	[39]
EBM Mean (Z)	119.2	[39]
SLM as-built (XY)	109.2	[51]
SLM heat treated (XY)	114.7	[51]
DMLS as-built	112	[8]
DED as-built	119	[47]
DED heat treated	118	[47]

The heat treatment for SLM which showed the best result, and is shown in Table 2.2 and 2.3, was 2 hours at 850 °C followed by furnace cooling. The improvements were an increase in the elastic modulus by 5.5 GPa and an increase in ductility by 5 %, at a cost of lowered yield strength.

2.6.2 Fatigue Properties of Additive Manufactured $TiAl_6V_4$

The current research into fatigue life of AM $TiAl_6V_4$ shows inconsistent results [47]. A lack of test standards together with varying fabrication methods and post processing methods create varying results and gathering a conclusive data is therefore difficult. However, something that is apparent is that occurrence of defects can significantly decrease the fatigue life. For example, Liu *et al.* [33] performed fatigue testing on SLM samples with a stress level of 600 MPa and received results varying from 10^4 to 10^6 cycles to failure due to defects. In the following paragraphs fatigue data for DED, SLM, DMLS, and EBM that have been heat treated and machined are presented.

DED samples subjected to HIP treatment for 2 hours at 900 °C and a tensile stress of 100 MPa displayed fatigue properties similar to wrought $TiAl_6V_4$ [30], see Table 2.4. At the stress amplitude 900 MPa the samples could withstand more than 10^4 cycles and at 800 MPa up to 10^5 cycles. The fatigue life displayed some anisotropic properties with lower fatigue life in the vertical build direction. Samples that were stress relived in vacuum for 20 hours at 700 °C displayed a significant anisotropy and a fatigue strength similar to or worse than cast material.

Table 2.4: Fatigue data for DED, machined, HIP [30]

Cycles	Stress Amplitude (MPa)
30 000	900
150 000	800
1 000 000	750

Zhao *et al.*[58] conducted fatigue studies on SLM samples, see Table 2.5. The stud-

ies were conducted with a R-ratio[2] of 0.1. Their conclusion is that heat treatment greatly increase the fatigue life of SLM produced samples achieving a fatigue limit above 550 MPa. The low fatigue limit of non heat treated SLM samples was attributed to a large amount of pores.

Table 2.5: Fatigue data for ASTM E466 SLM, machined, HIP, R-ratio 0.1 [58]

Cycles	Stress Amplitude (MPa)
1 000 000	700
2 000 000	600
10 000 000	575

Greitmeier *et al.*[24] conducted studies on $TiAl_6V_4$ produced by DMLS, see Table 2.6, and found that machining affects the fatigue to a larger extent than the method for heat treatment. HIP treatment displayed an insignificant increase in fatigue performance compared to annealing in the as-built condition and a slightly larger improvement in the machined condition. The HIP treatment was at 920 °C and 1000 bar for 2 hours under argon atmosphere and the annealing process was at 710 °C for 2 hours under vacuum followed by argon atmosphere cooling.

Table 2.6: Fatigue data for ASTM E647 DMLS, machined, HIP, R-ratio 0.1 [24]

Cycles	Stress Amplitude (MPa)
80 000	800
1 300 000	750
2 000 000	725
3 000 000	660
10 000 000	600
14 000 000	575

Greitmeier *et al.*[24] also conducted studies on $TiAl_6V_4$ produced by EBM, Table 2.7, with similar conclusions as for DMLS. However, in the machined condition the improvement of HIP over annealing was greater in the EBM samples than for DMLS samples.

Table 2.7: Fatigue data for ASTM E647 EBM, machined, HIP, R-ratio 0.1 [24]

Cycles	Stress Amplitude (MPa)
2 000 000	700
4 000 000	675
5 000 000	650
5 300 000	625
10 000 000	575
20 000 000	560

[2]R-ratio is the ratio of the minimum stress during a cycle to the maximum stress during a cycle.

2.7 Defects in Additive Manufactured $TiAl_6V_4$

AM is often characterized by defects as there are many process parameters that together will decide the properties of the printed metal. These defects can both be general for all additive manufactured materials or specific for certain AM methods.

2.7.1 General Defects

AM often comes with defects such as porosity. Small voids remain in the printed structure as a result of the melting of the powder. Generally there are two types of holes responsible for the porosity. Gas induced porosity is one type of defect where small holes filled with gas are created during the melting of the metal. These bubbles of gas are then trapped inside the material. Additionally, there are defects formed by the process technique, known as process-induced porosity. This occurs when insufficient energy levels for the melting are applied and results in partly unmelted powder grains or spatter ejection. Gas pores are typically spherical and pores formed by spatter ejection have more abstract shapes.

One key report in the subject of defects is written by Sames, *et al.* [40]. It presents several defects one may face when working with metal AM, such as Porosity, Rough surface, Residual stress, Delamination, and Swelling. Their results are used in the following two paragraphs.

Rough surface is one of the main problems when using AM methods and that it results in poor fatigue properties due to crack initiation if not dealt with. A simple solution to the problem is to machine the surface using Computer Numerical Control (CNC) mills, which requires printing a slightly larger model than what is actually needed.

Residual stresses, delamination, and swelling are defects that occur due to the melting process in AM. Residual stress is a stress within the material that remains after external loads are removed. These stresses are common in metal AM due to the large thermal gradients present. If the local stress exceeds the yield stress of the printed material, warping or plastic deformation may occur. If the stress exceeds the ultimate tensile strength cracks or other defects may occur. Delamination is the separation between layers within a part caused by incomplete melting between these layers. This can not be fixed in post-processing. Swelling is the phenomenon where solid material rises above the powder plane due to released stresses in the underlying layer.

2.7.2 Specific Material Defects for EBM and SLM

Gong *et al.* analyzed several defects that can occur during EBM and SLM processes [23]. The process parameters were altered to determine what parameters influenced different defects. They state, that for EBM manufactured $TiAl_6V_4$ the diameter of the beam, also called focus offset, that hits the powder can significantly affect the

final finish. For small focus offsets the laser penetrates the powder bed deeply and creates ridges, roughly 0.2 mm wide, resulting in a coarse surface finish. With an increase of focus offset the degree of surface roughness goes down. However, small half-spherical pores, up to 0.2 mm in diameter, might form. The pores could be due to molten powder releasing argon gas. If the focus offset is too great, voids may be generated due to a lack of melt pool overlap. This can also cause powder particles to not be melted. Further they tell, if samples are over melted pores can form in SLM samples as well. These pores are near spherical in shape and between 0.05-0.1 mm in diameter. The high solidification rate can cause defects within the material when entrapped gas does not have time to rise to the surface. These defects are near spherical with a diameter of around 0.1 mm with a surrounding keyhole geometry of martensite structure. If the melt is over irradiated molten material may be ejected to the surface creating solid particles that weld to the surface. These particles might be removed by the recoating blade and leave a pit with diameter of 0.03 mm. Using low energy density or large hatch spacing may result in no overlap between melted lines creating irregular voids and pores in the surface.

2.8 Heat Treatment

Research done on HIP treatment for SLM and EBM samples show that the treatment significantly improves the fatigue properties compared to as fabricated samples. This is credited to the pores in the micro structure being closed. For EBM and SLM without heat treatment the fatigue life was reduced with roughly 36 % and 40 % respectively. [58]

SLM samples, fatigue tested according to ASTM E466-07 [15], showed varying results depending on if heat treated or not [32]. The tests were done with an R-ratio of -1 at 600 MPa. An R-ratio of -1 is often called Fully Reversed due to the minimum stress being equal to the negative of the maximum stress. With no heat treatment the samples withstood 27.000 cycles and with HIP treatment they never failed at this stress level. Furthermore, the fatigue limit with HIP treated samples was then determined to 630 MPa. A characteristic of SLM is high temperature gradients. This results in faster solidification which in turn results in the build-up of internal stresses, and the presence of non-equilibrium phases in the micro structure. Because of this the fatigue properties of SLM $TiAl_6V_4$ can be an improved significantly using heat treatment [58].

A study from Greitemeier *et al.* [24] showed that different AM methods respond very differently to the same heat treatments. The study looked at samples from EBM and DMLS that were either annealed or HIP treated. The results showed that the fatigue life properties of DMLS were significantly more improved by HIP treatment while EBM showed comparably little difference between the two treatments. In their discussion they stated that this could be due to the absence of martensite in the micro structure and the forcibly dissolved alloying elements in the new structure of the HIP treated DMLS. The reason why this is not the case for EBM is said to

be a consequence of having a printing chamber with a temperature of about 630 °C. They also made the conclusion that fatigue life is dominantly influenced by process inherent surface roughness. They also show that if this is addressed, for example, by using milling, the fatigue life properties is mostly dependent on defects such as pores.

2.9 Surface finish

Process inherent surface roughness is the dominating factor when optimizing fatigue life properties. Hence, it is a necessity to take the machines settings into account becomes a necessity [24]. For example different SLM machines utilizes different fiber lasers and can be operated at various printing speeds. The laser offset can also be varied and a consequence of this is that the surface profile varies greatly depending on machine settings for the same method, see Figure 2.3. This also makes it possible to some degree decrease the surface roughness for some AM methods by modifying the machine settings [58]. However, modifying these settings will also result in changes in micro structure that might have a negative effect on the mechanical properties.

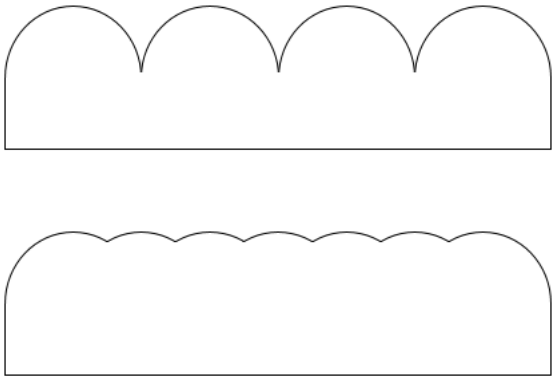

Figure 2.3: Simplified figure of process inherent surface roughness for different stages of melted metal powder. The above figure shows a lower degree of melt than the lower figure, resulting in a less clear separation between different powder spheres

2.10 Printing Direction

Edwards and Ramulu [19] studied the problems with fatigue assumptions regarding AM $TiAl_6V_4$. In their research they used an MTT 250 which utilizes SLM to evaluate if the fatigue properties vary between the different printing directions (x,y,z in a Cartesian coordinate system), where the z-direction is the vertical direction in the machine. Their tests are based on samples that have not received any post processing. The result of the study shows that while issues such as micro structure, porosity, surface finish and residual stress play the largest role in fatigue life, the

printing direction does matter. All samples (created in different directions) were tested to find the load that gave a life of 200 000 cycles. The samples printed in x-direction managed a load of 240 MPa on average, y-direction 170 MPa and the z-direction managed 100 MPa on average. The reason why it differs between x- and y-direction is because of how the laser moves over the powder as it melts it. Their conclusion from this is that there is a significant difference in fatigue properties in regards to printed direction.

There is an important difference between SLM and EBM; the electron beam in EBM rotates when printing which results in no difference in mechanical properties between x- or y-direction in the printed part. There is still a drop in fatigue properties in the z-direction in EBM [18].

2.11 Joining Techniques

During this project a lot of research has been put into finding machines that, using AM, can produce products of the size of the examined blisk. This has proven to be quite a challenge. The only currently existing machine able to create an entire blisk with a diameter of 1 meter, is Sciaky's EBAM 110 [42]. For details see Section 3.8.2. Additionally, this machine may not be suitable considering a variety of other factors, see Section 3.9.4. Therefore, it was determined that the blisk will have to be manufactured in pieces to be joined in an additional production step. Different joining techniques have therefore been evaluated. One may encounter problems when welding the blisk together because of the varying thickness in the disk section. This may force the manufacturer to use several welding techniques during the production process.

2.11.1 Gluing

Glue has been evaluated as a joining process. But after some research, it was found that there is currently no commercially available glue that can withstand the temperatures present in the blisk while maintaining its strength. In fact, no glue was found to provide sufficient strength for this application even in room temperature.

2.11.2 Electron Beam Welding

To weld different parts together into a blisk, a method called Electron Beam Welding (EBW) can be used. It works by sending a beam of electrons with high energy into the workpiece that melts. To prevent dissipation of the electron beam, EBW is usually performed under a vacuum [26]. When welding titanium alloys it is of great importance to avoid contaminating the heat effected zone and the fusion. Since EBW is performed in a vacuum, it will not let impurities to reach the metal. It also provides a weld with strength in line with the surrounding material [41], see Table 2.8. This table is based on two-pass double sided weld on a 17.5 mm thick plate. Compared to the AM methods previously evaluated, EBW is quick. With a speed of 1270 mm/min, 21 mm weld [41].

Table 2.8: Average material properties of EBW $TiAl_6V_4$ [41]

Ultimate Tensile Strength	Yield Strength	Elongation
988 [MPa]	930 (0.2 %) [MPa]	11 [%]

2.11.3 Laser Brazing

One method of joining that was investigated was laser brazing to connect the blades to the disk. Laser brazing is a joining method where the base metals are not melted but there is an introduction of a filler metal. This method can have a very high precision as well as a smaller heat affected zone. However, per a meeting with Penn State Material Science Professor Todd Palmer, laser brazing would not be suitable to join a $TiAl_6V_4$ blade to a $TiAl_6V_4$ disk hub as was requested for the project. Unalloyed Titanium and alpha Titanium alloys are possible to weld. However, when alpha beta alloys, such as $TiAl_6V_4$, are joined with another alpha beta alloy, the weld may be embrittled. [34]

2.11.4 Gas Tungsten Arc Welding

Gas Tungsten Arc Welding (GTAW), also known as Tungsten Inert Gas Welding, is a welding method which uses a non-consumable tungsten electrode and an inert shield gas. The shield gas prevents the metal from forming oxides and ensures no other impurities pollutes the material. A filler metal is normally used. This method was in a study regarding welding methods in $TiAl_6V_4$ and was determined to be the best option when welding plates only a few millimeters thick [54]. Eleven welding methods were compared in [54] and those can be found in the list below. However, it is not certain that GTAW will be the best welding method in this application.

- Gas Metal Arc Welding
- Gas Tungsten Arc Welding
- Plasma arc welding
- Electron-beam welding
- Laser-beam welding
- Friction welding
- Resistance welding
- Diffusion welding
- Explosive welding
- Brazing Welding
- Manual Metal Arc Welding

2.11.5 Linear Friction Welding

Linear Friction Welding (LFW) is a method used for joining two metal interfaces through solid state welding. This method of solid state welding provides a superior joint structure to fusion welding and can aid in increasing the reliability of the blisk.

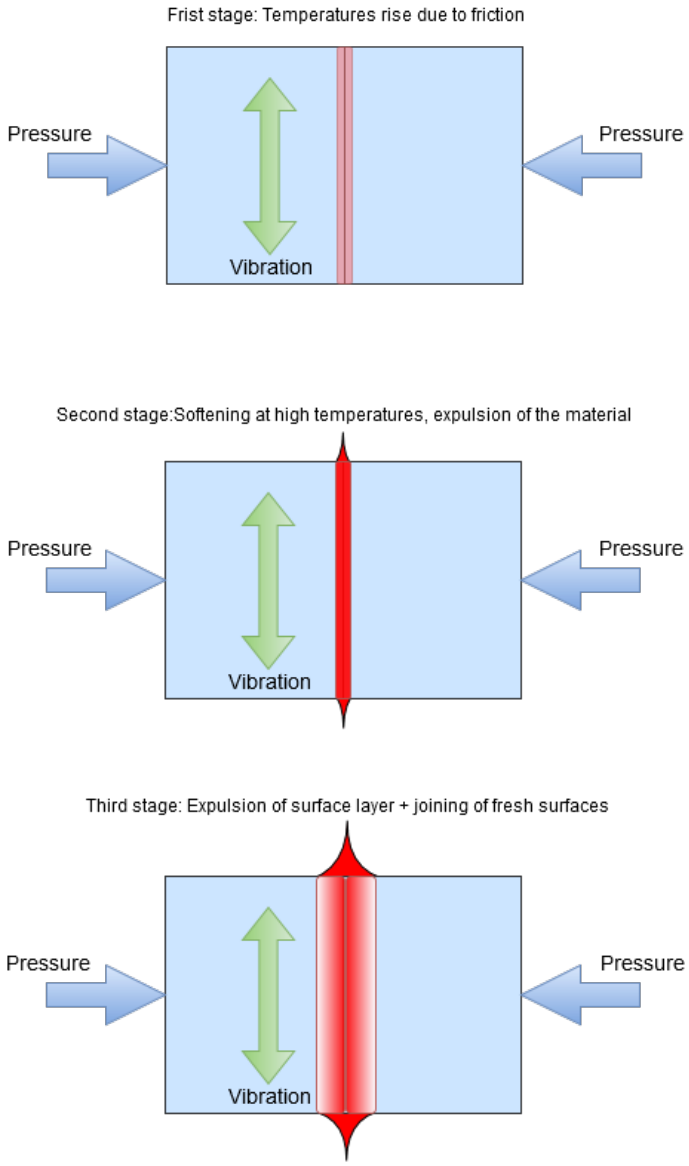

Figure 2.4: Three Stages of Linear Friction Welding adapted from [27]

As seen in Figure 2.4 LFW works by applying pressure to each side of the objects being joined, then moving one of the objects rapidly against the other in a parallel fashion to create heat from friction. This fuses the objects together [27]. LFW has been used previously to join machined blades to machined disks. This decreased the material waste of the process and reduced overall cost while achieving all necessary strength goals. The blisk created using LFW also passed all tests in relation to dimensional precision. [21]

2.11.6 Mechanical Joining Processes Today

In conventional compressor rotors the compressor blades are attached to the center disk using one of several different methods. Typically a dovetail style connection with a locking pin is used to secure the blades to the disk hub. Mechanical fittings

provide a more simple production process and easier reparations, but is less efficient when compared to a blisk. Since this project is focusing on creating a blisk with no mechanical fittings between blades and disk, these types attachment methods will not be evaluated further. There are numerous patents on these fittings. Some of the methods are briefly shown in Figures E.1, E.2, E.3, and E.4 in Appendix E.

3
Methods

In this chapter general project administrative matters are brought up, as well as methods used for evaluating materials and methods. This to ensure the ability to remake these studies if verification is needed. It is also a tool for the reader to evaluate the trustworthiness of this study.

3.1 Preliminary Economic Analysis for the Project

The total budget of the project was 1230 USD. This money was to be spent mainly on prototypes. PSU intended to, if possible, create a prototype in metal, and Chalmers would provide a prototype in plastic. Due to the cost of titanium AM methods, a different material was needed to be used for the metal prototype. The Bill Of Budget illustrates final expenses accrued by the team and can be found in Appendix A.

3.2 Project Management and Deliverables

A complete Gantt Chart can be found in Appendix D with tasks, subtasks, milestones, and deliverables. The Gantt Chart functioned as a living document and was updated as the project progressed. Additional tasks were added as needed and updates on existing tasks were made to reflect the accomplishments of the group. The use of a Gantt Chart kept an overview of the progression of the project, and brought attention to approaching deadlines. The overview also allowed team members to see if a specific task was not progressing as planned and required additional support. The Gantt Chart does not include who was responsible for each specific task. The division of specific minor tasks was done on a weekly basis. Larger tasks were divided as needed to complete their objectives in time.

The main responsibility of research on AM belonged to PSU as the group had better access to ongoing research and expertise in the field. Chalmers was responsible for simulations as the members had earlier experience and knowledge in finite element programs and its theory. Also, Chalmers offered access to a computer cluster for heavy simulations.

3.2.1 Deliverables

For additional information such as the start and finish date for project deliverables, see the accompanying Gantt Chart in Appendix D. A complete list of project deliverables is as follows:

- Weekly update memos for status reports
- Project proposal
- Additive manufacturing report
- Design report with technical specifications
- Finite element analysis report
- Full economic estimations
- Prototype
- Computer Aided Design (CAD) design of AM blisk or design of partly additive manufactured blisk including joining interface
- Final Report

3.3 Risk Plan and Safety

To minimize the negative outcome from potential risks within the project, a qualitative risk analysis was carried out at the beginning of the project timeline. In the risk analysis, potential problems and hazards are identified and their risk level defined. The actions that needed to be taken to minimize the probability of the risk are identified. In addition, a fall back strategy had been created in the event that the risk occurred. The objective was to identify potential hazards and minimize their effect on the project.

3.3.1 Risk Identification

Risks were identified through discussion with the team and sponsor. Areas where risks needed to be considered included: technology, scheduling, deliverables, project scope and reliability.

3.3.2 Risk Analysis

Once the risks were identified, their probability and impact had to be determined as low, medium or high.

The probability was set as follows:

- Low - Highly unlikely to occur. May occur in exceptional situations.
- Medium - Possible to occur.
- High - Highly likely to occur. Has occurred in previous projects.

The impact was set as follows:

- Low - Less than five extra hours work needed.
- Medium - Between five and ten extra hours work needed.

- High - More than ten extra hours work needed.

The combined result from impact and probability then determined the risk level. In the Impact-Probability table, Figure 3.1, red was high risk level, yellow medium risk level and green low risk level. In Table 3.1 a list of risks with impact and probability was compiled.

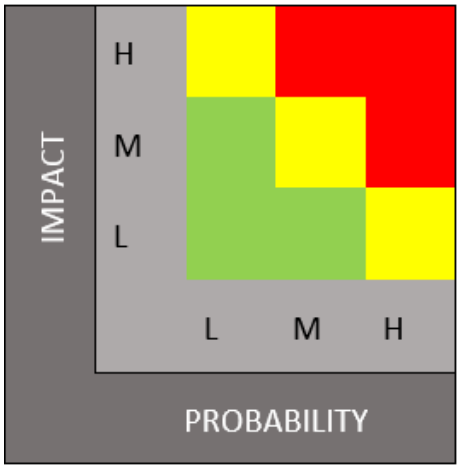

Figure 3.1: Illustrating risk level based on impact and probability

Table 3.1: Table of known risks

Risk	Impact	Propability
Project goals are too time consuming	High	Medium
Incorrect information results in unnecessary work being done	Medium	Low
Resources are inadequate	Medium	Low
The main goal of the project is incorrectly interpreted	High	Low
Poor communication results in double work	Medium	Low
Group members need to learn software they are unfamiliar with	Low	High
Loss of data	High	Low
Incorrect distribution of resources	Medium	Medium
Change to daylight saving dates do not match, resulting in missed meetings	Low	Medium
3D printers break	Medium	Low
Group members get sick	Low	Medium
Group members get very sick	High	Low

3.3.3 Risk Evaluation

To be as prepared against the risks as possible a Risk Plan Table was created, see Appendix B. In this table each risk was given a risk level that corresponded to its

impact- and probability level. The team discussed each risk and determined actions that needed to be taken to minimize its probability and impact. A strategy to be used if the risk occurs was also decided.

3.4 Ethics Statement

Throughout this project, it was the goal of the team to complete our tasks in a highly ethical manner. Specifically, the group abided by the code of ethics set forth by the American Society of Mechanical Engineers [10]. The final results of the project needed to ensure safety in manufacturing, testing, as well as operation and repair processes. All aspects of the project were completed with respect to GKN Aerospace's bladed disk standards to ensure it is compliant with the work they are doing at the company.

All research completed was properly documented using reputable sources and information that was used is properly referenced. The work that was completed by the team has been reviewed thoroughly and presented to GKN Aerospace. No unnecessary liberties were taken during the project's duration including, but not limited to, a disregard for safety regulations.

3.5 Environmental Statement

All team members pledged to complete this project in concurrence with all applicable environmental standards, such as ISO 14000. Through the use of AM, our group intended to reduce the unused material waste in the creation of the blisks and ensure it is done in a safe and effective manner. Each decision made that could have an environmental impact was discussed and approved by each member of the team as well as GKN Aerospace. The team strived to create a concept that has no adverse effects to the environment. All proposed processes were reviewed for their environmental impacts and if needed, the processes was modified to ensure there are no violations.

3.6 Customer Needs Assessment

This section specifies the customer needs on the product. It also specifies what needs should be focused on most on via the use of an AHP (Analytic Hierarchy Process) matrix Pairwise Comparison Chart.

3.6.1 Gathering Customer Input

After consulting with GKN Aerospace on their AM Initiative, the following list of objectives were generated.

- Reduce material waste
- Increase freedom of design
- Reduce production steps
- Safety
- Increase durability
- Reduced weight
- Develop clever and inexpensive repair methods

3.6.2 Weighting of Customer Needs

Considering the above mentioned objectives, an AHP matrix with weights, presented in Table 3.2, was created to provide information about the weight between different objectives, see Table 3.3. These objectives will from now on be called costumer needs.

Table 3.2: Weights in AHP Matrix

Weight	Equals
0.33	Much worse
0.5	Worse
1	Equal
2	Better
3	Much better

Table 3.3: AHP Pairwise Comparison Chart to Determine Weighting for Main Objective Categories

	1.	**2.**	**3.**	**4.**	**5.**	**6.**	**7.**	**8.**	**Total**	**Rel.**
1. Less Material	1	0.5	1	1	0.33	0.5	0.5	1	5.83	0.069
2. Freed. of Design	2	1	3	3	0.5	2	2	3	16.5	0.196
3. Production time	1	0.33	1	1	0.33	0.5	0.5	1	5.66	0.067
4. Production cost	1	0.33	1	1	0.33	0.33	0.5	1	5.49	0.065
5. Safety	3	2	3	3	1	3	3	3	21	0.250
6. Durability	2	0.5	2	3	0.33	1	2	3	13.83	0.164
7. Weight	2	0.5	2	2	0.33	0.5	1	2	10.33	0.123
8. Repairability	1	0.33	1	1	0.33	0.33	0.5	1	5.49	0.065

The results from the AHP matrix are shown in Table 3.4. It is established that safety is the most important aspect, as it should be since safety is the number one concern with airplane engines, followed by Freedom of Design. Repairability, production cost, and production time ended up weighing the same as less material. This weighing of costumer needs is supported by GKN Aerospace.

Table 3.4: Results from AHP

Safety	0.250
Freed. of Design	0.169
Durability	0.164
Weight	0.123
Less material	0.069
Production time	0.067
Production cost	0.065
Repairability	0.065

3.7 Mechanical Analysis of AM Methods

To get results regarding the practical differences in the blisk using different AM methods, several simulations were performed using the different material properties presented in Table 3.5, 3.6, 3.7, and 3.8. The information neded for these simulations is presented here.

3.7.1 The Evaluated Blisk

Exact dimensions is considered confidential information so no exact dimensions will be displayed. The blisk is about one meter in diameter and weighs roughly 40 kilograms, with $TiAl_6V_4$ as the chosen material. It has 75 blades and each blade is about 100 mm long. The shape can be seen in Figure 3.2.

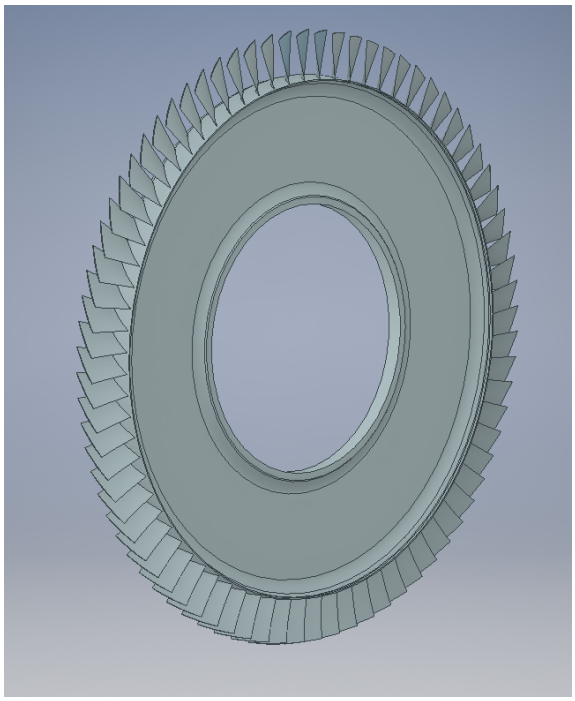

Figure 3.2: Shape of evaluated blisk

3.7.2 Material model

When creating the material input for simulation of the different AM methods the values stated in Section 2.6.1 were used. Due to limitation of available data, not all necessary properties could be found. Therefore, this section goes through the simplifications and assumptions that were made of the material parameters in ANSYS[6].

Since the material properties vary depending on the printing direction, orthotropic elasticity properties were chosen for the different models. Input data for this is Young's modulus in x-, y-, z-directions, Poisson's ratio, and shear modulus in the xy-, yz- and xz-planes. The assigned values for Young's modulus can be found in Table 2.3. The issue of limited available data comes in when assigning values to Poisson's ratio and shear modulus. This is because the current research in AM materials has not yet been confirmed for all properties and specifically not in different printing directions. Therefore, the ANSYS models have been assigned the lowest values of standard $TiAl_6V_4$ in the cases that specific values for AM could not be found. This resulted in a Poisson's ratio of between 0.34 och 0.36 and a shear modulus of 40 GPa for all models [49].

The fatigue data from Section 2.6.2 was implemented in ANSYS. As stated in Section 2.6.2 fatigue life depends on a multitude of aspects and has a recorded variance depending on its orientation when created, defects, and its exposure to loads. However, today's research of mechanical properties of AM $TiAl_6V_4$ has not yet reached a point where reliable data for AM $TiAl_6V_4$ is available. The results from the fatigue analysis must therefore be analysed with skepticism.

Due to the relatively early stage of current research into mechanical properties, the correlation to temperature is not available. A consequence of this is that all material properties in the ANSYS models are for a material at 22° C. All of these things will have to be considered when analyzing the result of the simulations. The material parameters used in the simulations in ANSYS can be found in Table 3.5[1], 3.6[1], 3.7[1], and 3.8[1].

[1] **Interpolation:** Linear interpolation between datapoints regadring fatigue data using linear axes.

Table 3.5: Material parameters for machined EBM

Property	Value	Unit
Density	4430	kg/m^3
Young's modulus x-direction	114.4	GPa
Young's modulus y-direction	114.4	GPa
Young's modulus z-direction	119.2	GPa
Poisson's ratio xy	0.34	
Poisson's ratio yz	0.34	
Poisson's ratio xz	0.34	
Shear modulus xy	40	GPa
Shear modulus yz	40	GPa
Shear modulus xz	40	GPa
Alternating stress R-ratio	See Table 2.7	
Interpolation	Linear	
Tensile yield strength	975	MPa
Tensile ultimate strength	1023	MPa

Table 3.6: Material parameters for machined SLM

Property	Value	Unit
Density	4430	kg/m^3
Young's modulus x-direction	109.2	GPa
Young's modulus y-direction	109.2	GPa
Young's modulus z-direction	109.3	GPa
Poisson's ratio xy	0.36	
Poisson's ratio yz	0.36	
Poisson's ratio xz	0.36	
Shear modulus xy	40	GPa
Shear modulus yz	40	GPa
Shear modulus xz	40	GPa
Alternating stress R-ratio	See Table 2.5	
Interpolation	Linear	
Tensile yield strength	1060	MPa
Tensile ultimate strength	1200	MPa

Table 3.7: Material parameters for machined DMLS

Property	Value	Unit
Density	4430	kg/m^3
Young's modulus x-direction	112.0	GPa
Young's modulus y-direction	112.0	GPa
Young's modulus z-direction	109.3	GPa
Poisson's ratio xy	0.36	
Poisson's ratio yz	0.36	
Poisson's ratio xz	0.36	
Shear modulus xy	40	GPa
Shear modulus yz	40	GPa
Shear modulus xz	40	GPa
Alternating stress R-ratio	See Table 2.6	
Interpolation	Linear	
Tensile yield strength	967	MPa
Tensile ultimate strength	1131	MPa

Table 3.8: Material parameters for machined DED

Property	Value	Unit
Density	4430	kg/m^3
Young's modulus x-direction	118.0	GPa
Young's modulus y-direction	118.0	GPa
Young's modulus z-direction	118.0	GPa
Poisson's ratio xy	0.34	
Poisson's ratio yz	0.34	
Poisson's ratio xz	0.34	
Shear modulus xy	40	GPa
Shear modulus yz	40	GPa
Shear modulus xz	40	GPa
Alternating stress R-ratio	See Table 2.4	
Interpolation	Linear	
Tensile yield strength	850	MPa
Tensile ultimate strength	920	MPa

3.7.3 ANSYS Setup

To perform the simulations in ANSYS the simulation model had to properly created. A boundary condition was set, loads were implemented, and the CAD model was meshed.

The model had a single boundary condition. The inside of the rotor, marked by blue in Figure 3.3, is fixed.

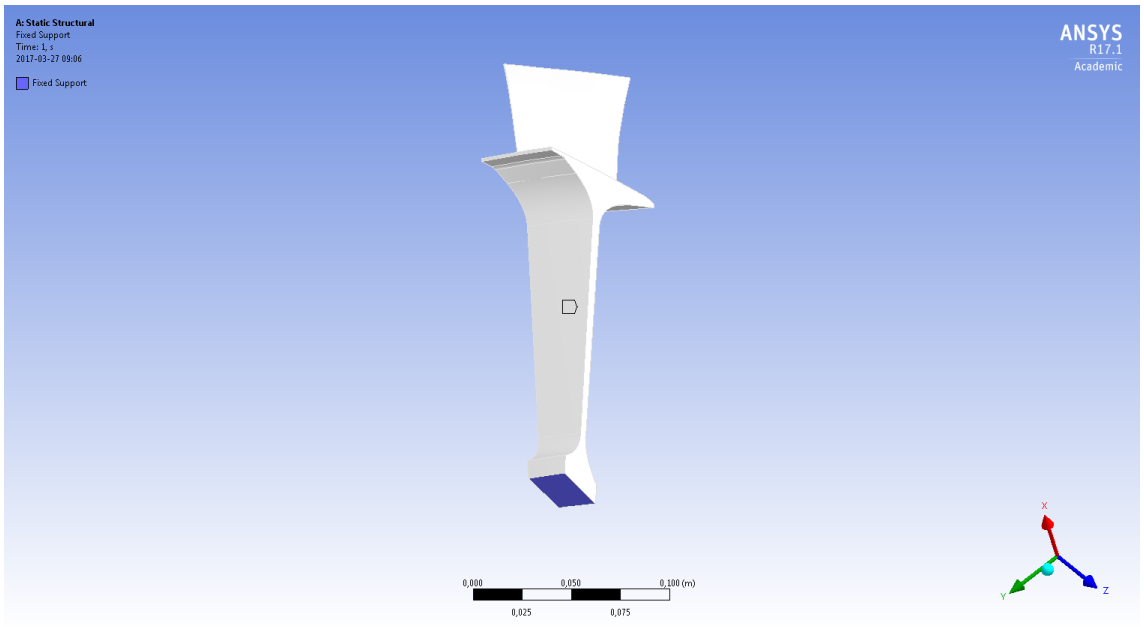

Figure 3.3: Boundary condition of blisk in ANSYS

The model was subjected to three loads implemented in ANSYS, as specified by GKN Aerospace. The rotational velocity ω and the pressure p can be seen in Figure 3.4, marked by yellow and red respectively. The values for all three loads are given in Table 3.9. For the fatigue analysis the values in Table 3.9 were used and for the stress analysis the presented values + 15 % were used.

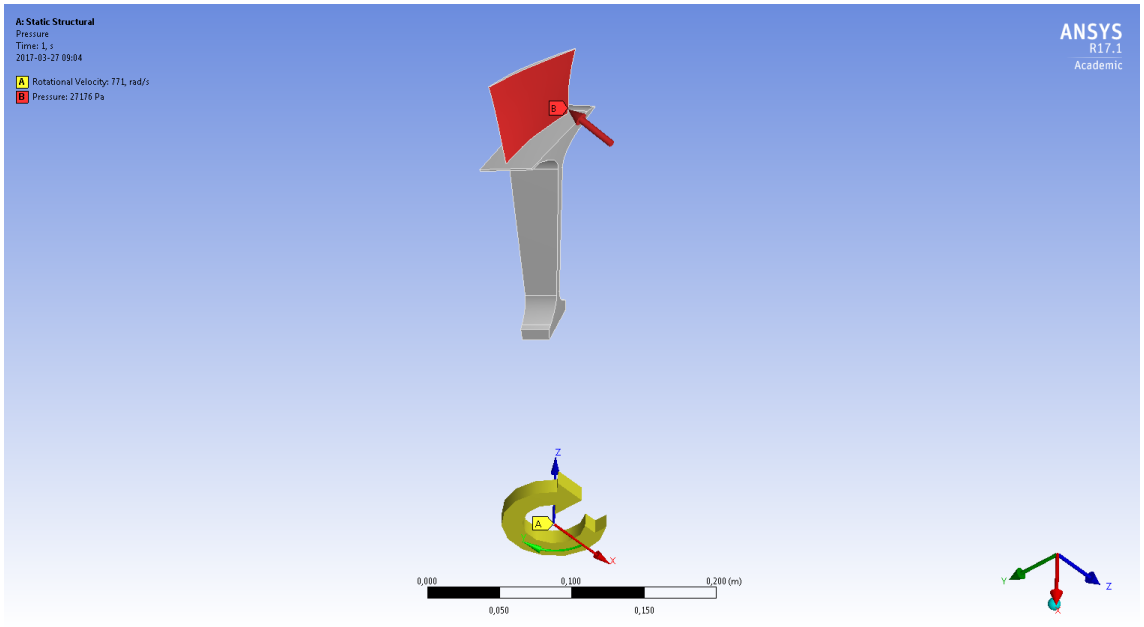

Figure 3.4: Rotational velocity and pressure as load on blisk in ANSYS

Table 3.9: Implemented loads in ANSYS

Load Type	Load
Rotational velocity	771 rad/s
Temperature	459 K
Pressure	27176 Pa

The pressure on the blades were calculated from the work the blisk performs, which was given by GKN Aerospace. The following formulas were used to calculate the pressure:

The blisk power is given by

$$P = M\omega \tag{3.1}$$

where M is the moment and ω is the rotational velocity.

The moment on the blisk is given by

$$M = F_{\text{tan}} r \tag{3.2}$$

where F_{tan} is the tangential force on the blade and r is the radius to the centre of the blade.

The force normal to the blade, by component separation, is given by

$$F_{\text{normal}} = \frac{F_{tan}}{\sin(\alpha)} \tag{3.3}$$

where α is the angle between the axial and tangential direction.

The resulting pressure on the blade is given by

$$p = \frac{F_{\text{normal}}}{A_{\text{tot}}} \tag{3.4}$$

where A_{tot} is the total area of all the blades.

For the stress analysis, the body of the rotor was meshed coarsely with an element size of roughly 0.015 m as these parts are more uniform and therefore easier to compute on. However, because of their complicated shape, the blades were meshed finely with an element size of 0.003 m. Furthermore, the outer surface of the rotor was meshed with an element size of 0.005 m. The mesh can be seen in Figure 3.5. This mesh size was found to be appropriate after performing a convergence test with finer and finer mesh until the stresses converged with an accuracy of 5 %.

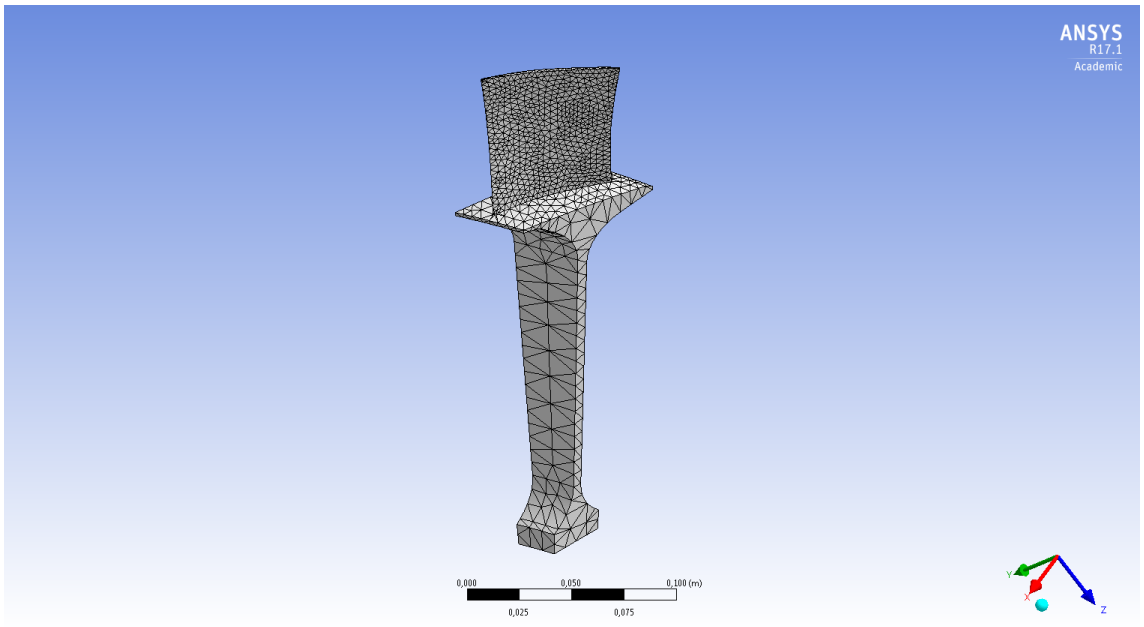

Figure 3.5: Mesh of blisk for stress analysis

The fatigue analysis was done on the entire blisk, therefore requiring more computational power, a more coarse mesh was used for this analysis. The average element size for this mesh was 0.025 m, see Figure 3.6.

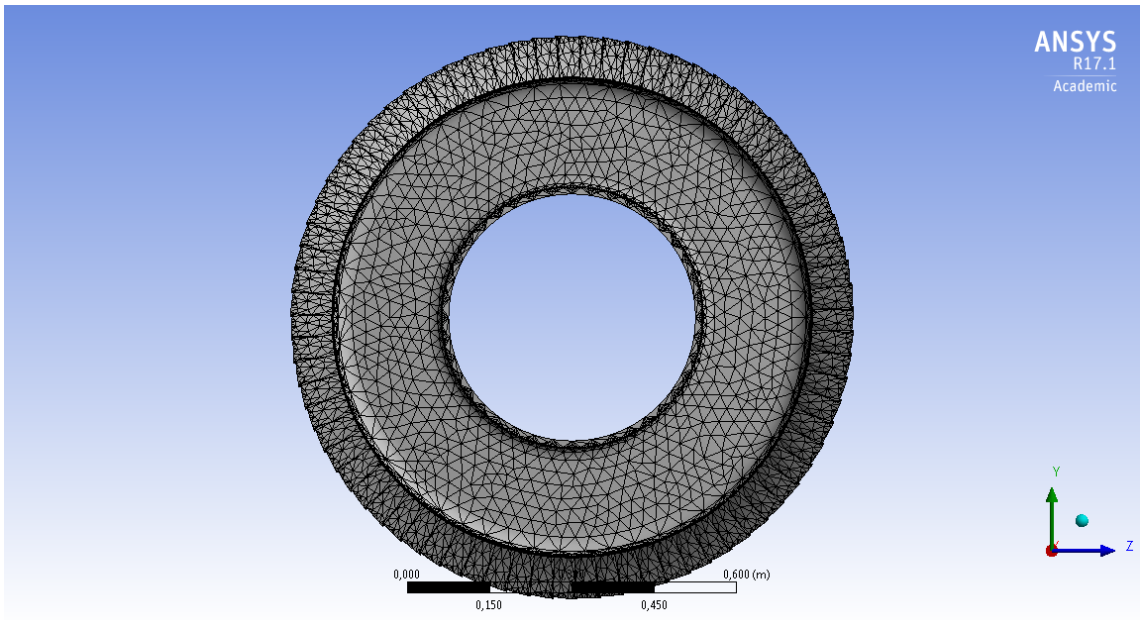

Figure 3.6: Mesh of blisk for fatigue analysis

3.8 Additive Manufacturing Application to Project

As previously stated throughout the report, the two sections of AM methods being investigated are Powder Bed Fusion and Direct Energy Deposition.

3.8.1 Powder Bed Fusion (PBF)

Examples of PBF manufactured parts can be found in Section 2.3.1 and include Airbus Defense and Space's Titanium Satellite Clamps as well as GE Aviation's Engine Fuel Nozzle. With the given dimensions of the blisk it was apparent that the size would be an issue for PBF machines. Currently, according to the Senvol Database [5], the largest PBF machine has a build platform of 500 mm x 400 mm x 350 mm. The blisk has a diameter of 1100 mm so a print in its entirety will not be possible with these methods.

While the blisk can not be printed in its entirety, PBF machines could still be used if printing the blisk in parts. For example, printing the blades and hub separately and then joining them together. An alternative would be to print circle sectors of the blisk and join these.

3.8.2 Direct Energy Deposition (DED)

DED has multiple applications that could be applicable for this project. One such application could be to be used to repair blisks. Companies such as Optomec and Huffman have exhibited success with using DED to repair blisks made from $TiAl_6V_4$. Through testing using LENS created by Optomec, material properties were found to be equal or better when compared to the base material. Through DED and proper finishing, this system could be applicable for GKN Aerospace for repairing damaged blisks [48].

Direct energy deposition could also be applicable for the creation of the blades of the blisk. One of the most wasteful aspects of blisk creation is the formation of the blades due to their geometric properties and the inherent restrictions of machining. Similar to the joining method mentioned above, the disk could be created through existing machining methods. Following the creation of the disk, it could be mounted in a DED machine. The blades could be formed as the disk was rotated until all blades are created. A single layer would be applied to each individual blade as the blisk was being rotated. This would avoid any issues that could occur due to the DED head interfering with the last blade as it is being created. Machining would then to occur to maintain tolerances and surface finish as DED would create only a near net shape. Unlike PBF, there are multiple machines that have build volumes large enough to fit the blisk in its entirety. Example such as Sciaky's EBAM 110, 150, and 300 systems are all able to fit the 1100 mm diameter blisk [43].

Companies like Tekna specialize in the development of variations of the pack density and sphericity of molecules within the powder for different applications. During an interview, Tekna provided the team with information brochures designed for assessing quotes of customers that described different grades, apparent densities beginning at 2.2 g/cm^3, are created by plasma atomisation for use in different components in

the aerospace industry including blisks.[2]

DED technology has been increasing in performance substantially in the past few years. A study conducted at the Oak Ridge National Laboratory ran a laser at 300 W which produced a scanning speed of 13.12 mm/s and a volumetric powder flow rate of 12.5 g/min [36]. The end result of this experiment produced hatch spacing of 0.46 mm and layer spacing of 0.30 mm [36]. A more recent study claims that DED has reached a max volumetric powder flow deposition rate of 41.579 g/min using steel as the medium [57].

One issue to consider with DED are the physical attributes of the individual powder spheres. Upon deposition, the spheres can impact one another which causes a different trajectory than the intended printing location. A CFD simulation was composed in 2014 to determine the inconsistency of particle trajectories. The max irregular trajectory velocity of a particle was found to be 10 m/s [56]. This model was developed with an input of powder flow rate of 100 g/h. The scattering of particles will increase with the faster the deposition rate. Modern DED machines have been rated at up to 700 g/h and sometimes even faster which could lead to further trajectory losses.

Four major leaders in the DED industry offer their systems for purchases and can be seen below in Table 3.10. Notably, Optomec offers solutions specifically for blisk repair with their Laser Engineering Net System (LENS) process.

Table 3.10: Leading Vendors

Vendor	Model	Dimensions (mm)[of working envelope in chamber]
DMG Mori [35]	LASERTEC 65	735 x 650 x 560
Optomec [37]	LENS 850-R	900 x 1500 x 900
Sciaky [43]	EBAM 300	5791 x 1219 x 1219
BeAM [11]	Magic 2.0	1200 x 800 x 800

3.9 Concept Generation

The project's main objective was to evaluate the possibility of creating a blisk using AM that fulfills the requirements of today's blisks. To accomplish this, an extensive external search has been performed as well as mechanical and economical analyses. The results from these have been used to evaluate different AM and joining methods.

3.9.1 Concept Limitations

A consequence of the project's main objective is that no mechanical joining methods will be evaluated as this would conflict with the objective. Furthermore, all concepts

[2]Phone call with Tekna representatives, March 19 2017

that were initially considered were selected based on their potential capabilities of solely printing the entire blisk using AM methods. Hybrid approaches where part of the blisk was machined using contemporary methods whilst other components of the blisk were printed via AM methods were not considered.

3.9.2 Evaluation of Build Speed

In determining build speed for a blisk using AM methods, there multiple factors had to be considered. The numerous manufacturers and machines have different build speeds for different reasons. Factors that must be considered, depending on the AM method chosen, include: nozzle temperature, material, layer thickness, number of supports required, desired quality, and laser power among others. For this reason, it can be difficult to calculate an exact production time.

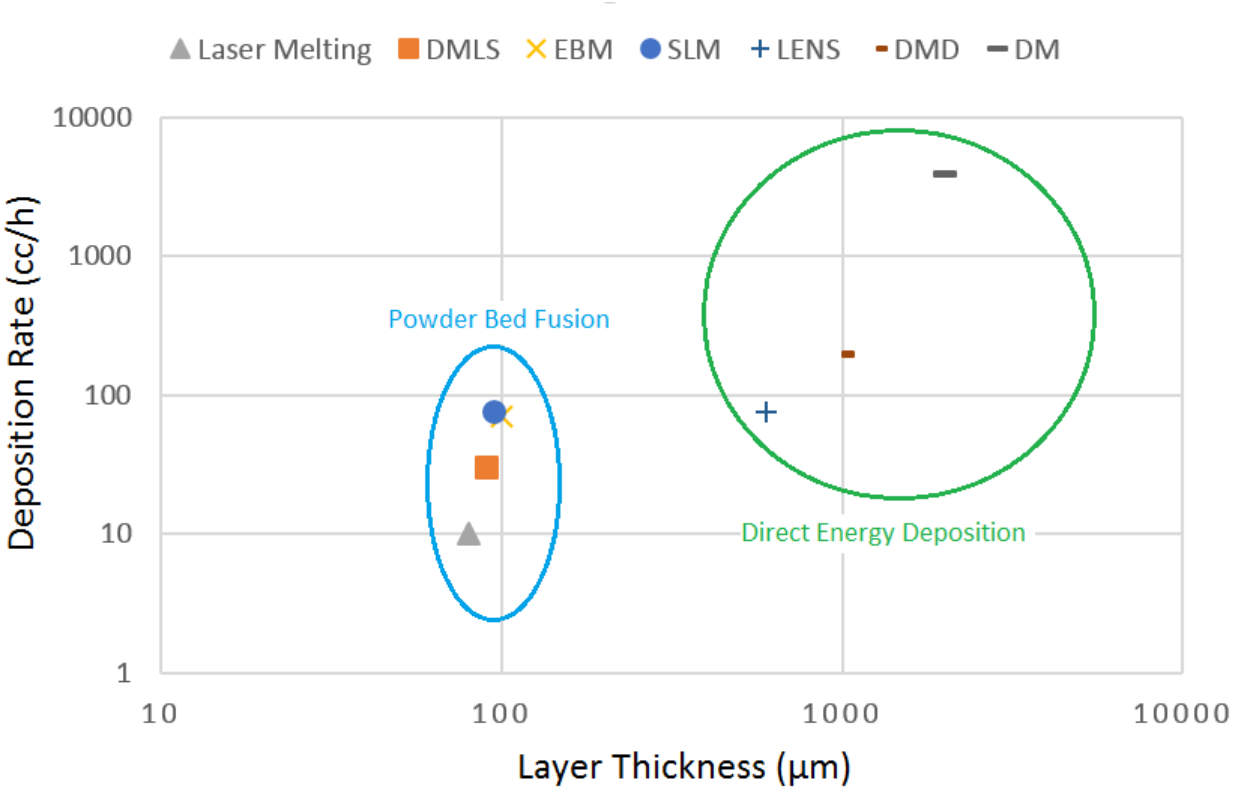

Figure 3.7: Comparison of build speed for DED and PBF adapted from [16]

As seen in Figure 3.7, it is apparent that DED machines print much faster when compared to PBF methods. However, upon further examination it is evident that DED has a much greater layer thickness than PBF. This leads to less detail and a higher degree of surface roughness.

Table 3.11 shows an average build speed and other features associated with different AM methods based on multiple manufacturers and studies.

Table 3.11: Characteristics of Relevant AM Methods

Characteristic	DMLS	EBM	SLM	DED
Build Envelope	Limited	Limited	Limited	Large and Flexible
Layer Thickness	Small 0.1-0.5 mm	Small 0.2-1.0 mm	Small 0.02-0.1 mm	Large 2.0-4.0 mm
Build Speed	Low 80-110 g/hr	Low 220-300 g/hr	Very low 4-40 g/hr	High 500-800 g/hr
Surface Finish	Good	Good	Very Good	Coarse

As can be seen in the above table, certain methods allow for faster production, making them more desirable. Also, long production time can lead to increased risk factors. For instance, if the machine was to lose power for any reason, calibration would likely be affected and the piece would not finish properly. Another risk associated with slow build speeds is the chance of contaminants causing a defect in the part. With limited ability to review the build as it is happening, defects would likely not be caught until the print has been completed, causing further delay in production time [14].

It is clear that DED machines are much faster than PBF machines; however, it should be noted that due to the rougher surface finish of DED methods, there would likely be an increase in post-machining required leading to an increase in production time. It should also be noted that due to the size of the blisk, it cannot be printed in its entirety. Due to this fact, additional time must be accounted for joining methods of the AM blades to the machined disk hub.

3.9.3 Evaluation Process

Different concepts will be created based on the different AM methods, joining processes and heat treatments. The relevance and quality of a concept will be evaluated based on data presented in Chapter 2. They will be evaluated using weighted Pugh decision-matrices and the proven best concept will be our final concept and chosen method. Weights to the Pugh decision-matrices are based on Table 3.4.

First off the AM methods SLM, DMLS, EBM, and DED were evaluated. They are evaluated in Table 3.12 and 3.13 in Section 3.9.4. Second comes the joining methods. EBW, GTAW, Laser Brazing, and LFW were used here and can be found in Section 4.2.2. They are evaluated as a complement with the proven best AM method in Section 3.9.4. The heat treatments HIP and annealing was examined last in Section 4.2.1, based on Section 2.8. A short discussion about post process machining can be found in Section 4.2.3. The purpose of post process machining is to enhance surface roughness which will greatly improve the fatigue properties.

3.9.4 Evaluation of AM Methods

Table 3.12 and Table 3.13 are created using a scale 1 to 5 (R column), with weighted results in the following column (W column). The best AM method according to Table 3.13 is EBM, it scored highest when evaluated to the weights in the AHP matrix in Chapter 3.6. It also scored second in Table 3.12, after SLM which scored a lot worse than EBM in the second table. The ratings of the material properties in Table 3.13 are based on the result of Table 3.12. The customer need "Durability" was not evaluated as there is no metric to compare methods. Additionally "Safety" was not evaluated as there is no distinguishable difference between methods. Finally, "Production cost" was not evaluated as no data for this criteria was available.

Table 3.12: Pugh matrix of AM methods based on material properties

Properties		**SLM**		**DMLS**		**EBM**		**DED**		**Notes**
	Weight	**R**	**W**	**R**	**W**	**R**	**W**	**R**	**W**	
Yield strength	2	5	10	3	6	4	8	3	6	Chapter 2
Elastic modulus	1	4	4	4	4	5	5	5	5	Chapter 2
Fatigue	3	5	15	5	15	5	15	5	15	Chapter 2
Total			29		25		28		26	
Rating			1		4		2		3	

Table 3.13: Pugh matrix of AM methods

Properties		**SLM**		**DMLS**		**EBM**		**DED**		**Notes**
	Weight	**R**	**W**	**R**	**W**	**R**	**W**	**R**	**W**	
Freed. of Design	3	4	12	5	15	4	12	2	6	Chapter 2
Less Material	1	3	3	3	3	5	5	5	5	Chapter 2
Prod. Time	1	0	0	2	2	4	4	5	5	Chapter 2
Mat. Properties	2	5	10	4	8	5	10	4	8	Chapter 2
Total			25		28		31		24	
Rating			3		2		1		4	

4
Results

Each manufacturing method were evaluated in ANSYS[6] using the material models introduced in Section 3.7.2. The result showed that the effective stresses in the models are far below the yield stresses for all methods. Furthermore, the fatigue analysis showed that there is no risk for fatigue failure if the surfaces are machined and the material heat treated.

4.1 Results from Mechanical Analysis in ANSYS

Several analyses in ANSYS were performed to evaluated the stresses, fatigue life, and the eigenfrequency of the blisk for the different AM-methods.

4.1.1 Results from Stress Analysis

Stresses are evaluated to identify where the loads affect the design the most. This is critical to gain an understanding of where failures are likely to occur and which parts are most vulnerable to crack initiation. The most important aspect of the stress evaluation is to verify that the effective stresses is not larger than the ultimate tensile strength of the material, as this would imply a fracture. Because the stresses in this problem are mainly affected only by forces and geometry, almost statically determined problem, the stresses will not differ much between the current blisk design with wrought $TiAl_6V_4$ and the different methods with additive manufactured $TiAl_6V_4$.

As can be seen in Figures 4.1 and 4.2 the surface of the blades are subjected to stresses of up to roughly 150 MPa. As expected there are some stress concentrations where the blades attach to the surface of the rotor due to the lack of fillets in the model. Theoretically with an infinitely small mesh size these stresses would be infinitely high.

The middle part of the disk experience stresses ranging from 10 MPa to 360 MPa, see Figure 4.4 and 4.3. The rotation of the blisk creates a centrifugal force which cause these stresses.

The highest stresses occur on the outside of the surface of the rotor, labeled Max in Figure 4.1, where the stresses reach 550 MPa. The stresses are higher on this side

of the rim due to an imbalance in mass distribution between the front and back of the rotor. The side with the higher amount of mass will experience higher stresses due to higher centrifugal forces.

To validate the stresses computed by ANSYS, calculations in a simplified case were performed. The calculations were performed as rotating circular disk with constant thickness.

Radial stresses

$$\sigma_{\mathrm{r}} = A - \frac{B}{r^2} - \frac{(3-\nu)\rho\omega^2 r^2}{8} \tag{4.1}$$

Circumference stresses

$$\sigma_{\varphi} = A + \frac{B}{r^2} - \frac{(1+3\nu)\rho\omega^2 r^2}{8} \tag{4.2}$$

Radial displacement

$$u_{\mathrm{r}} = \frac{1}{E}\left(A(1-\nu)r + \frac{B(1+\nu)}{r} - \frac{(1-\nu^2)\rho\omega^2 r^3}{8}\right) \tag{4.3}$$

where A and B are constants, ρ is the density, ν is Poisson's ratio, E is the elastic modulus, and ω is the rotational velocity.

The boundary conditions used were $\sigma_{\mathrm{r}}(b) = 0$ and $u_{\mathrm{r}}(a) = 0$ where a is the radius to the inner rim and b the radius to the outer rim.

The von Mises equivalent stress was then calculated as $\sigma_{\mathrm{vM}} = \sqrt{\frac{1}{2}[(\sigma_{\mathrm{r}} - \sigma_{\varphi})^2 + \sigma_{\mathrm{r}}^2 + \sigma_{\varphi}^2]}$ and were found to be 90 MPa at a distance of 0.3 m from the centre of the disk which is in the same order of magnitude as the results from ANSYS.

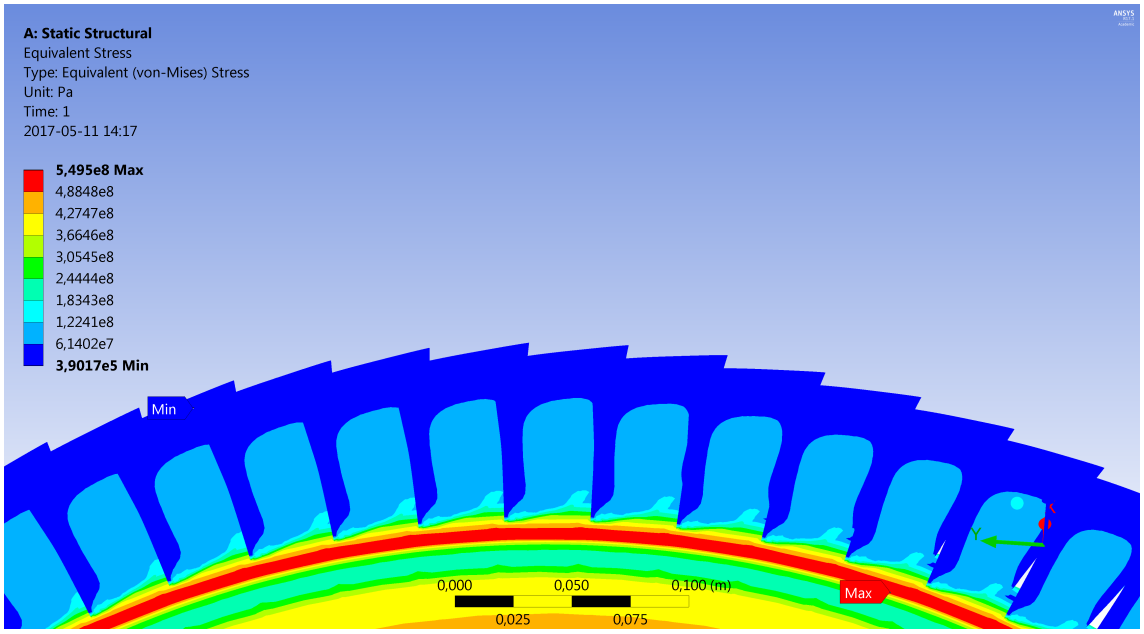

Figure 4.1: von Mises stresses on opposite side of pressure load

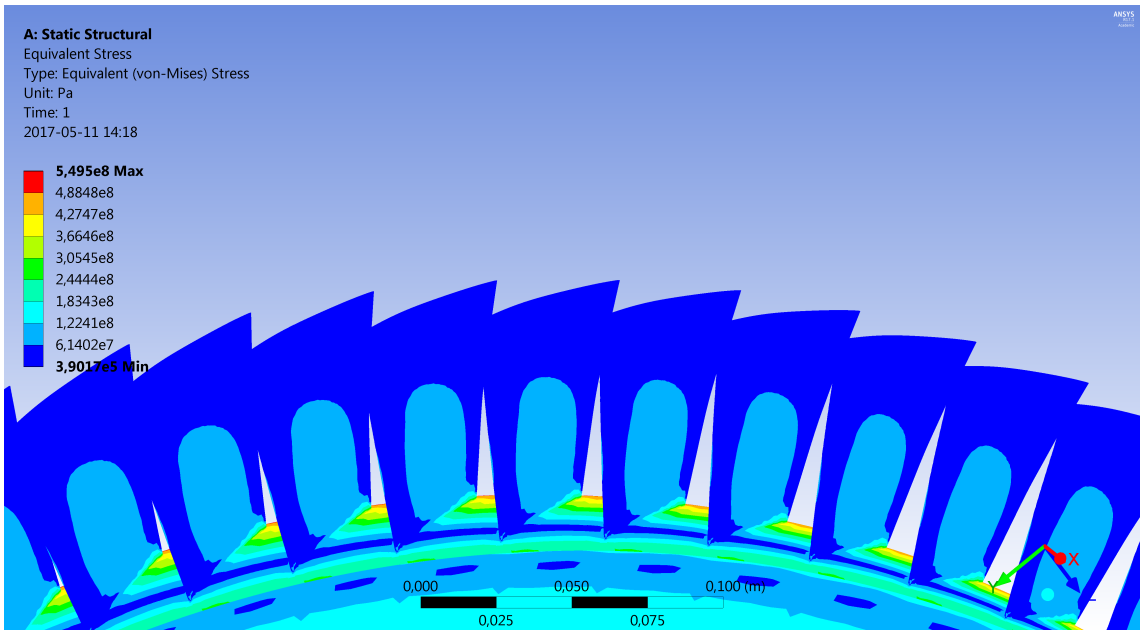

Figure 4.2: von Mises stresses on same side as pressure load

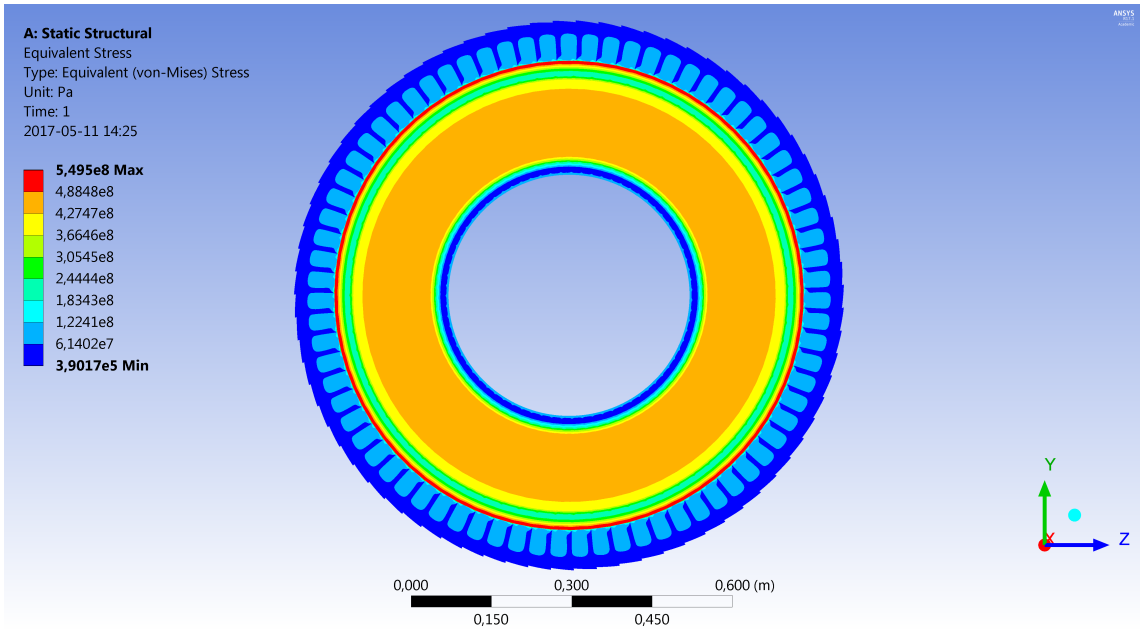

Figure 4.3: von Mises stresses on the front of body

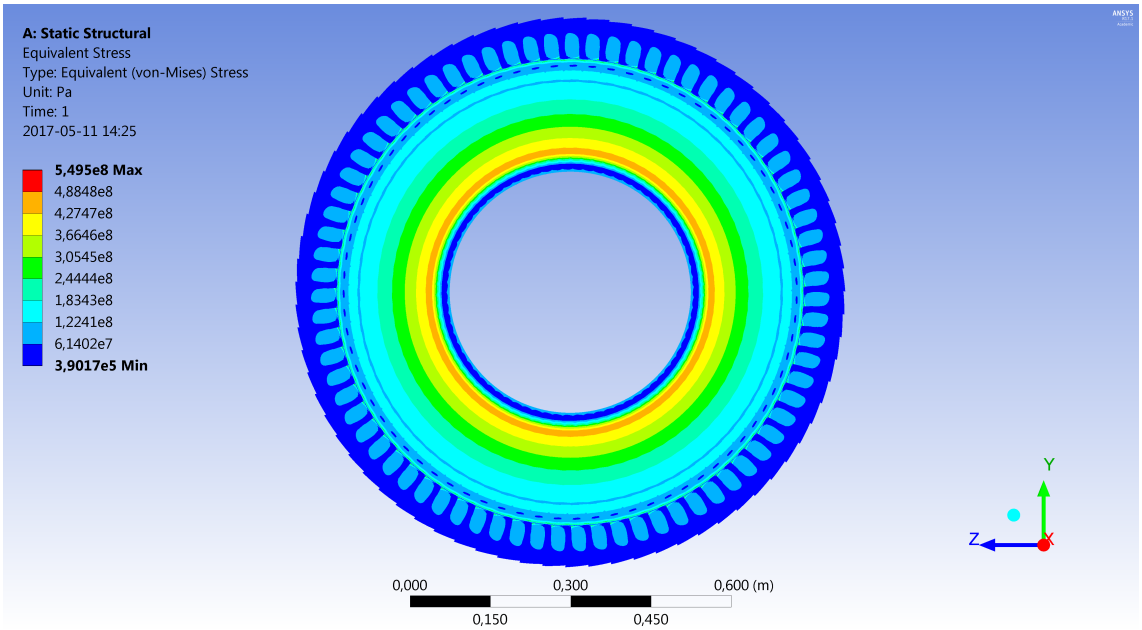

Figure 4.4: von Mises stresses on the back of body

4.1.2 Results from Fatigue Life Analysis

The blisk is subjected to cyclic loading since it is started and shut down repeatedly more than 10 000 times. Therefore, high cycle fatigue has to be analysed. Because the data in Section 2.6.2 is for smooth samples, a fatigue strength factor must be implemented in ANSYS. This factor takes into account differences between the samples used in the fatigue data and the actual design [48]. The fatigue data should be reduced by the following factor

$$\frac{\lambda}{K_f K_d K_r} \tag{4.4}$$

where λ, K_f, K_d, and K_r are non dimensional reduction factors depending on material, loads, and geometry.

The reduction factor λ is only applicable to cast products and is therefore set to 1. The factor K_f is used to take into account stress concentrations which is something ANSYS implement automatically so the factor is set to 1 with an understanding that the material is taken to be sensitive to stress concentrations. Furthermore, the geometric factor K_d is also set to 1 due to only being applicable in applications with bending or torsion. Finally, the surface factor K_r is used to take into account surface roughness of the model. The factor is available for steel at different experimental ultimate tensile stresses and values for surface roughness (R_a). Since λ, K_f, and K_d is set to 1 the fatigue data should therefore only be reduced with the surface roughness factor $1/K_r$, as given in Table 4.1. Using a reduction factor $1/k_r = 0.75$ means the fatigue data is reduced by 25 %.

Table 4.1: Reduction due to surface roughness for steel with UTS of 1000 MPa [48]

R_a (μm)	$1/K_r$
20	0.575
10	0.625
9	0.63
8	0.635
7	0.64
6	0.655
5	0.65
4	0.675
3	0.685
2	0.8
1	0.83

Fatigue analyses were performed in ANSYS by increasing the reduction incrementally from zero until the model could withstand 30 000 cycles as requested from GKN Aerospace. The different methods could withstand being reduced with a factor ranging from 76 % to 65 %. The fatigue results from all four methods are presented in Figures 4.5, 4.6, 4.7, and 4.8. As anticipated the minimum life was always observed in the rim with the maximum stresses. The method that could withstand the most amount of reduction was DED with 76 %, closely followed by DMLS with 74 %. EBM managed 70 % reduction and SLM 65 %. With these results the blisk would be able to withstand the cyclic loads even if it had a very large inherent surface roughness.

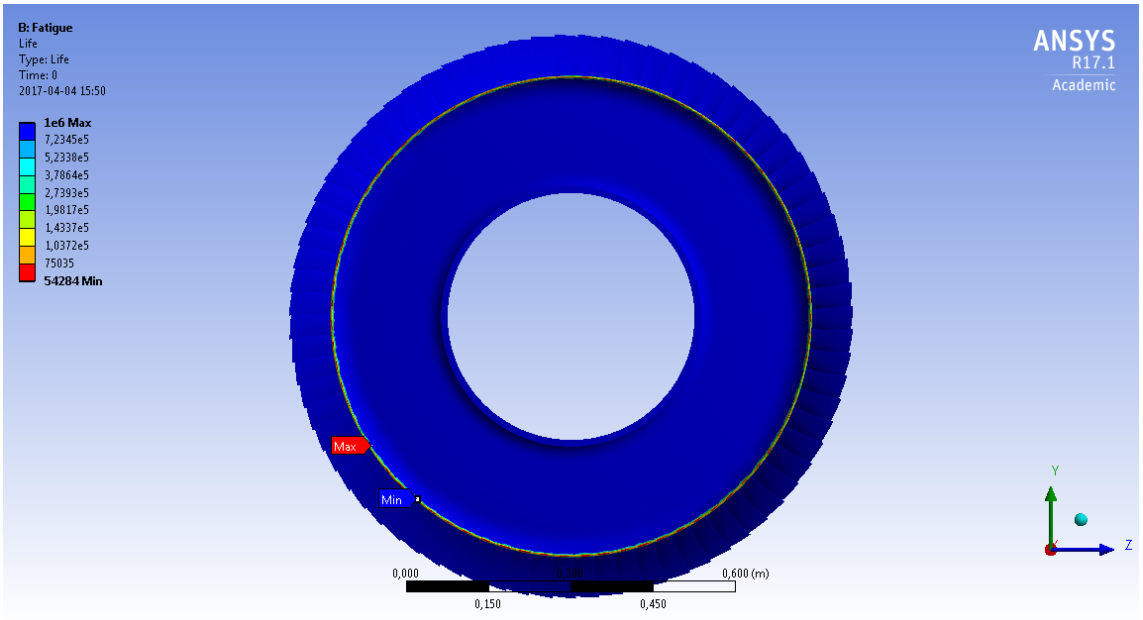

Figure 4.5: Fatigue life with DED and reduction factor of 0.24

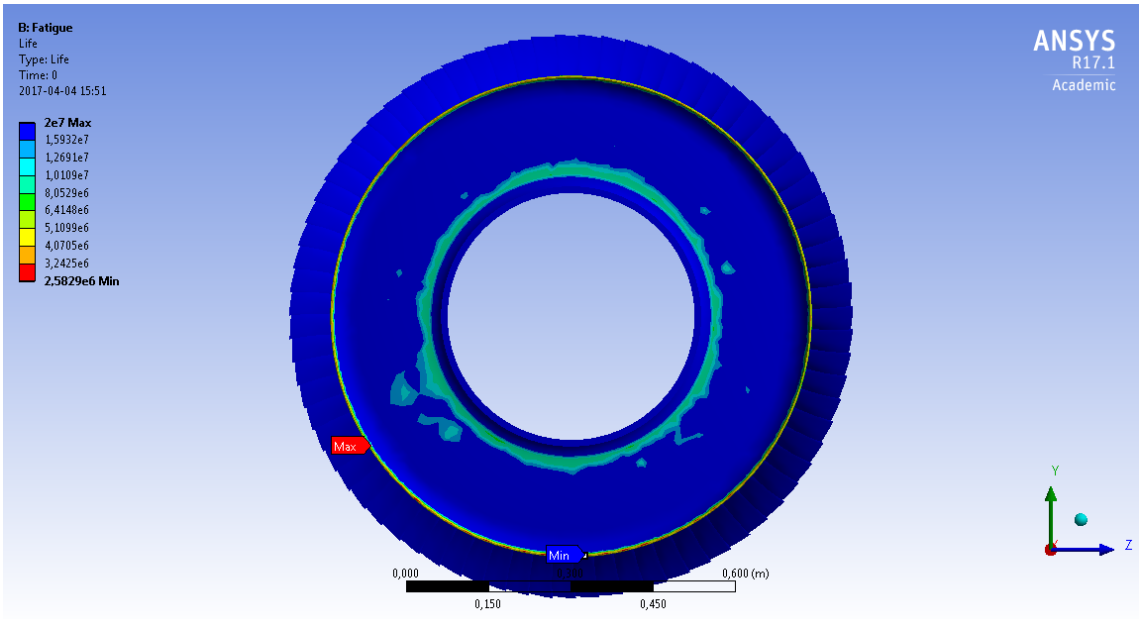

Figure 4.6: Fatigue life with EBM and reduction factor of 0.30

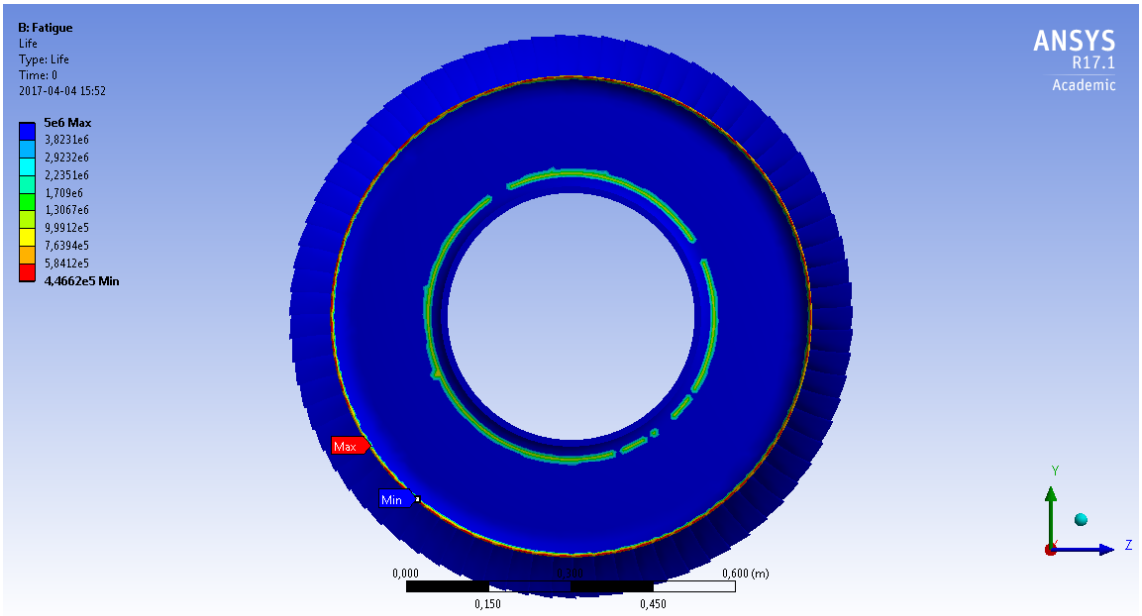

Figure 4.7: Fatigue life with SLM and reduction factor of 0.35

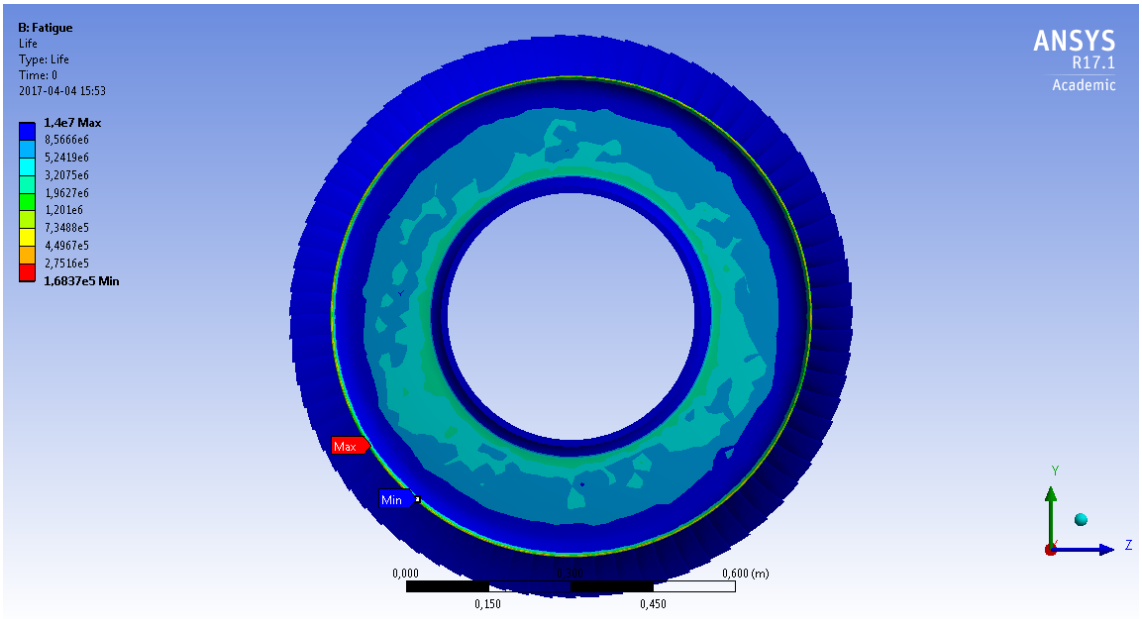

Figure 4.8: Fatigue life with DMLS and reduction factor of 0.26

4.1.3 Results from Deformation Analysis

When designing a blisk two models are created; a warm model and a cold model. The warm model has the desired dimensions for optimum performance during operation. The cold model are then designed in a way so that when applying the loads to the cold model it will be deformed into the dimensions of the warm model.

The given geometry is the warm model, meaning it is dimensions are as it would be during operation and the deformations are already implemented in the CAD model. Because of this, no deformation analysis will be done as those simulations should be performed on the cold model.

4.1.4 Results from Campbell Diagram

A Campbell diagram was requested by the GKN representative. This diagram presents the relation between eigenfrequency and rotational velocity. The intersections between the modal lines and the rotational velocity line mark the critical speeds. These critical speeds are to be completely avoided or quickly passed when reaching supercritical speeds[1]. Otherwise the rotational speed and eigenfrequency will match and escalating oscillations may occur. The examined blisk has an operational rotational velocity of 771 rad/s.

Campbell diagrams and corresponding tables were made for the blisk using ANSYS tools and are presented in Figure 4.9, Table 4.2 and in Appendix F. The six first frequencies were analysed and all used material parameters presented in Section 3.7.2 were tested. Figure 4.9 and Table 4.2 was created without pre-stresses. The purpose

[1]Rotating faster than the first critical speed.

of them is to compare it to the ones created with pre-stresses, which can be found in Figure F.1 and Table F.1.

The actual rotational velocity of 771 rad/s on the rotors, is not dangerously close to a critical speed. However, regulations on safety factors probably exist regarding these matters. These regulations have not been checked.

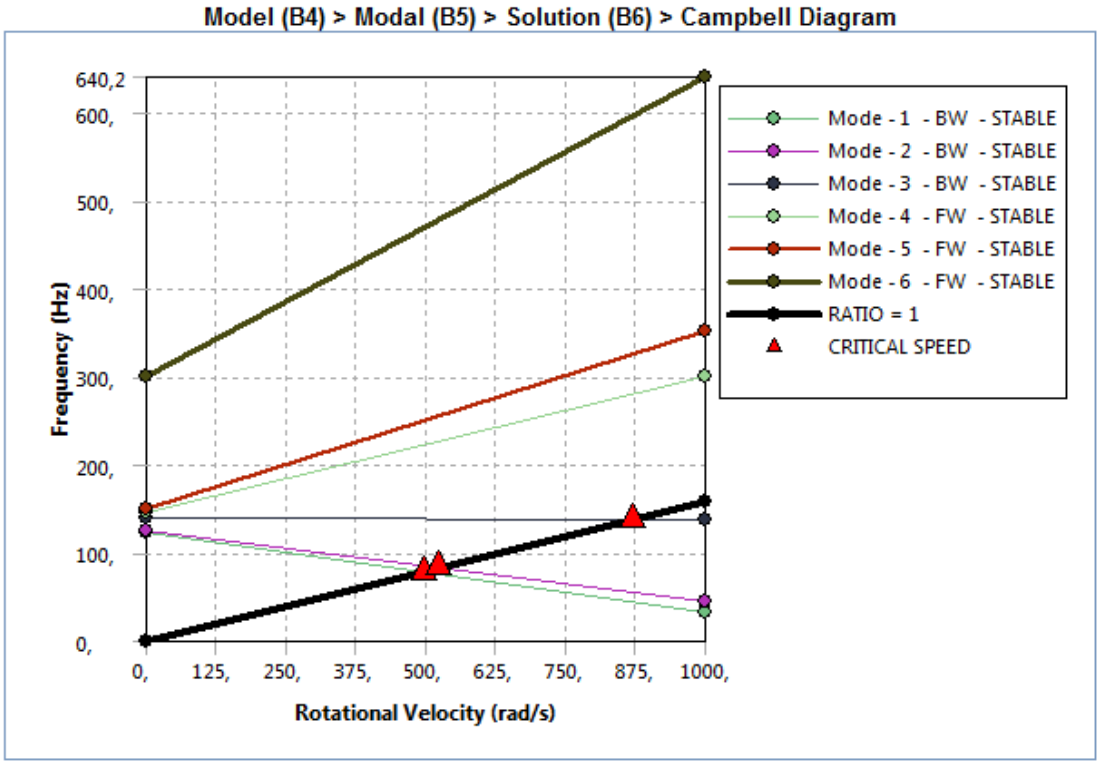

Figure 4.9: Campbell diagram without pressures on the blades with machined EBM, see Table 3.5

Table 4.2: Campbell table without pressures on the blades with machined EBM, see Table 3.5. The last two columns tell the eigenfrequency for respective mode in Hz for the blisks rotational velocities 0 rad/s and 1000 rad/s.

Mode	Whirl Dir.	Mode Stab.	Crit. Speed	0, rad/s	1000, rad/s
1	BW	Stable	495,51 rad/s	123,94 Hz	32,971 Hz
2	BW	Stable	524,24 rad/s	124,59 Hz	46,087 Hz
3	BW	Stable	869,91 rad/s	139,45 Hz	138,3 Hz
4	FW	Stable	0 rad/s	146,49 Hz	299,82 Hz
5	FW	Stable	0 rad/s	150,35 Hz	352,58 Hz
6	FW	Stable	0 rad/s	299,88 Hz	640,2 Hz

4.2 Concept Selection

Based on the theory in Section 2 the final concept was chosen. When the final concept had been chosen an economic analysis is conducted to determine the feasibility of the concept.

4.2.1 Evaluation of Heat Treatments

When searching for heat treated AM samples two options were found, see Section 2.8. There is a possibility that other treatments might work as well or even better but only data for HIP and annealing were found. There is also an option to not use any heat treatment, which gives three options in total that can be evaluated. Research stated in Section 2.8 shows that when comparing treated samples to not treated samples the treated ones show more favorable mechanical properties. The next step becomes to evaluate which of the two treatments that is better. The research that the project has studied shows that there were no case where HIP was found to be the less favorable. In some cases HIP and annealed were found to be too close in properties to state as one superior, as was the case for EBM. As HIP treated EBM samples often received better properties and closes pores this method was chosen.

4.2.2 Evaluation of Joining Methods

There is slight obscurity in the selection of a joining method due to the nature of the project. With the variable selection of AM method research and selection, not very substantial time was devoted to determining a joining method as any slight variation in the AM process selection would significantly change which joining method would be used and how. Despite this approach, some promising techniques was found and one of them is EBW, see Section 2.11.2. EBW provides welding for relatively thick parts and it automatically provides shielding from impurities and oxidation, due to the vacuum. One issue that arises with EBW would be creating a container which can hold a vacuum large enough to contain the entire blisk. Additionally, laser brazing was also ruled out as it could not join two $\alpha + \beta$ alloys together. LFW gives great strength in the weld and is fast and efficient, but it requires simple geometries, which denies some of the freedom of design. GTAW is a well established method when welding with high precision. The source used in Section 3.9.2 did the testing on plates only a few millimeters thick and got great results. The depth to which GTAW can be used and possibly other critical data is however unclear and should be investigated further.

EBW is, based on these presented arguments as well as recommendations from GKN Aerospace, chosen as the best welding method for this application. Especially since it provides great welding in thick parts with high accuracy.

4.2.3 Evaluation of Post Process Machining

To ensure sufficient surface finish without sacrificing any mechanical properties by altering the process parameters, the final concept will include CNC milling and/or finishing machining. In the production process of a blisk at GKN today, three steps of machining exist. If the net shape of the blisk after EBM printing is good enough, the two first steps might be avoided.

4.2.4 Final Concept

EBM has been presented to be the best AM method for the application of this project. It is clear that if no modifications to the current machines are made, the blisk will have to be printed in multiple parts to be assembled later. Great results could be reached if an EBM machine large enough to print an entire blisk is created in the future. If the machine could print the entire blisk at once, there would be no need to print it in pieces. This would eliminate the need for joining techniques and further simplify the process.

The blisk could be printed in fifteen circle sectors with five blades each, which should later be welded together using EBW. The number of sectors will differ depending on the size of the blisk, but for the size of the project specific blisk, 15 sectors was found to be optimal with Arcams Q20 printer in mind. After welding, the blisk needs to be heat treated using HIP. This heat treatment should then be followed by a final surface finishing to ensure sufficient surface condition. The use of EBM and EBW combined to produce a blisk is the final chosen concept.

4.2.5 Comparable Economic Analysis of Chosen Concept

GKN Aerospace supplied the project with a cost estimate for manufacturing the blisk using conventional machining as well as a cost model calculating the cost of the chosen concept with EBM. EBM costs were calculated for an Arcam Q20 machine printing 8 sectors with 5 blades each of the blisk. The model includes machine costs, labour costs, and manufacturing costs. When comparing the total cost for conventional machining to the total AM costs, the conventional costs will be set to a base value of 1 and all the AM cost will be presented relative to this cost.

The cost for conventional manufacturing, see Table 4.3, is divided into material cost and all other costs which include machining, heat treatment, inspections, and labour.

Table 4.3: Breakdown of costs when using conventional manufacturing methods

Cost item	Percentage of total cost
Material	60
Other costs	40

In Table 4.4 a breakdown of AM costs is displayed. A notable figure is the manufacturing cost, where material cost make up 90 % which is roughly 45 % of the total production cost. The AM cost only includes a HIP treatment and no machining or welding.

Table 4.4: Breakdown of costs when printing the chosen concept in an Arcam Q20 EBM machine

Cost item	Percentage of total cost
Machine	37
Labour	13
Manufacturing	50

With conventional production methods the machining is divided into three steps: rough machining, semi-finishing machining, and finishing machining. The Arcam Q20 machine would provide a sufficient surface finish to only need the finishing machining. This step makes up roughly 70 % of the total machining time based on figures provided by GKN Aerospace. Assuming machining makes up 70 % of the "other costs" for conventional manufacturing the relative cost for the finishing machining is roughly 20 % of the total cost for conventional manufacturing ($0.4 \times 0.7 \times 0.7$).

When comparing AM to conventional production methods, see Table 4.5, AM would cost 24 % more than conventional machining when not including the finishing machining. When including the finishing machining using AM would cost 44 % more than conventional manufacturing methods. Although these figures are neither exact nor including all costs they give a rough estimate for the cost of utilizing AM to produce the blisk compared to using the conventional method.

Table 4.5: Relative cost of Arcam Q20 to conventional machining

Production method	Relative cost to conventional manufacturing
Conventional manufacturing	1
Arcam Q20	1.24
Arcam Q20 + finishing machining	1.44

5
Discussion

A general theme throughout the external search was the uncertainty of data. Several sources contradicted each other and there was no general consensus on terminology, making it difficult to get an in depth and accurate understanding of the underlying theory. Furthermore, the status of current research has not yet reached a point where it is detailed enough. Additionally no officially recognised data is available for fatigue, temperature dependence, and influence of varying process parameters. This created difficulties when evaluating and comparing AM methods.

Due to the uncertainty of data collected during the external search, results from ANSYS must be reviewed thoroughly. Most importantly, the large variety of process parameters in addition to varying test methods make the data regarding fatigue properties unreliable. However, the results from ANSYS showed the fatigue data could be reduced by a substantial amount and still the blisk could withstand 30,000 cycles. This result implies that the fatigue properties would be sufficient for the project even if the actual fatigue properties would be significantly worse than the data gathered. Furthermore, the evaluation of AM methods in respect to fatigue life were limited. Due to the fatigue data not being detailed enough, difficulties arose when evaluating the fatigue life in ANSYS as the few amount of data points made comparisons between AM methods unfeasible. There were in many cases as few as 4-8 samples tested in total for an S-N diagram. To put that in perspective, to have an accuracy of 50 % about 20 samples are needed. But due to the cost of one AM sample of $TiAl_6V_4$ and the cost of test machines, most studies simplify. This means most of the available research needs to be critically reviewed.

Sharp corners in the model can cause stresses in the area to approach infinity as the element size approaches zero, according to the linear elastic model. These high stresses cause plastic deformation in the model when they surpass the yield stress limit of the material. The effect of this has not been evaluated. However, it could have been interesting for the project as the request of 30,000 cycles also could be evaluated using low cycle fatigue theory where plastic strain is a central aspect.

One may notice that the distribution of fatigue life results is not symmetric in Figure 4.6. This may be an effect of the mesh not being symmetric. The mesh is not symmetric as there was a problem in ANSYS that prevented fatigue calculations when using cyclic symmetry. This meant that a rougher mesh needed be used on the entire blisk and therefore the unsymmetrical result could appear.

Most studies only test the elastic modulus in the xy plane and the z direction. However, there could be differences in x and y direction as well. A difference between elastic moduli of x and y directions, when printing a part with rotational symmetry, can cause problems as the deformations would not be uniform in the radial direction. This could lead to an imbalance in the part.

Due to a slight change in elasticity modulus between additively manufactured and wrought $TiAl_6V_4$, the cold model has to be changed to maintain the specified design of the warm model.

An aspect of this project was evaluating a variety of joining methods. Linear Friction Welding was one such method that could be promising, depending on the application. In the case that each blade was printed individually, using EBM, it could be attached to a previously machined disk using LFW. Because there was a limitation regarding time in the project, this welding method were not thoroughly evaluated. However, it has shown promising results in the past and could very well be a good solution.

Due to the relatively new nature of these systems, it was very difficult to complete a detailed and accurate economic analysis. When researching, very few studies discuss the topic of price as the technology is still in its relative infancy. Some work regarding the economics have been done in close contact with GKN Aerospace, which gave some basic results. The main goal of this project was to evaluate the feasibility of AM technology in the application of the blisk. This coupled with the relatively low importance of cost as a customer need forced us to spend more time evaluating different AM technologies.

As AM continues to progress, many new technologies are being created that could apply to the production of a blisk. The biggest limitation that was faced was the size of the blisk. There are currently no PBF machines on the market that have a build envelope large enough for the blisks proposed. As technology progresses, larger build envelopes are sure to be constructed. These technologies could allow the blisk to be printed in its entirety.

6
Conclusion

Several conclusions about how a AM printed blisk should be manufactured can be drawn from the content of this study. The proposed method is to use EBM to print circle sectors of the blisk, as they would then be able to fit in the build envelopes of available machines. Following the completion of the print, EBW should be used to join each of the sectors. The blisk will then need to be heat treated through an HIP process, and then undergo a surface finishing procedure to meet all surface finish tolerances. While it could not be printed in its entirety, this process allows AM to be used to entirely create the blisk. Based on ANSYS simulations, the strength and fatigue life where found to be comparable to currently machined blisks. The concepts and ideas for GKN Aerospace is presented in the list below:

- Additive manufacturing has been found to be a suitable production method for blisks. Both PBF and DED machines can create a material and design that are sufficient for the application. Although DED is the only method capable of printing the blisk in its entirety, the low amount of freedom of design for DED makes it unsuitable. This method would require a large mount of support structures.

- The best method after evaluations was determined to be EBM. EBM would offer a large amount of design freedom, low material waste, relatively quick production, and good mechanical properties.

- No EBM machine capable of printing the entire design exists. The blisk will therefore be printed in 15 circle sectors of five blades each, and then joined together.

- The best welding method for joining the circle sectors together was found to be EBW. EBW is able to weld parts of varying thickness with great precision.

- Heat treatments are required to receive fatigue properties that are sufficient for the project. Without heat treatments the mechanical properties are unreliable due to pores and other defects in the additive manufactured part. The suggested heat treatment is HIP.

- A Campbell diagram was created to analyze the relationship between eigenfrequencies and the rotational velocity. By examining the tables and figures in section 4.1.4, the operational rotational speed of 771 rad/s was found to not be dangerously close to any critical speed.

- Through many simulations in ANSYS, it is evident that the AM blisks had fatigue lives far above 30,000 cycles. These simulations were evaluated using documented material properties for EBM, DSLS, SLM, and DED.

7

Self Assessment

This chapter discusses how well this project has followed the customer needs presented in Table 3.4 in Section 3.6. It also brings up how the project team has performed regarding environmental and ethical matters, as discussed in Section 3.4 and 3.5.

7.1 Customer Needs

On a scale of 1-10, where 10 is fulfilling all customer needs, this project gets a 9.33 from the group. This is because all needs were fulfilled except for reducing the production time of the blisk, which had a low AHP rating. The number was calculated by summarizing the AHP values of all fulfilled costumer needs from Table 3.4.

Safety is the most important aspect according to Table 3.4. Therefore all AM methods have been carefully evaluated in ANSYS to make sure they perform well enough to meet standards. Since safety factors are met by all methods, the main focus went from safety to freedom of design. It had the highest weight in Table 3.13. One may argue that material properties could be translated to safety. The reason material properties has a lower weight than freedom of design is because the material properties of the different AM methods were very close to each other.

7.2 Global Needs

Since all extra objectives stated in Section 3.4 and 3.5 have been fulfilled, the group gives itself an 8 out of 10 for meeting global needs. Due to the fact that the project has not done a complete Life Cycle Analysis, it can not give itself a 10 because it does not know the full environmental impact of the new blisk compared to the old one.

All sources used have been critically reviewed and deemed as trustworthy enough for this project. Biased sources have, to the greatest extent, been avoided. Throughout the project, two smaller presentations and a continuous conversation have been held with GKN Aerospace to ensure that the project proceeded as planned, did not deviate from its objectives or that the final concept exceeded the tolerances.

Environmental effects have not been the main focus, instead the focus has been on improving the blisk. An improved blisk could possibly increase the efficiency of a jet engine, which in turn could reduce harmful emissions. Also, reduced material waste in the production would contribute to a more environmentally friendly product.

References

[1] Blisks. http://www.gkngroup.com/aerospace/products-and-capabilities/engine-rotatives/blisks. Online; accessed 2-March-2017.

[2] Compressor and turbine blades & vanes. http://www.gkngroup.com/aerospace/products-and-capabilities/engine-rotatives/compressor-blades. Online; accessed 2-March-2017.

[3] Dmls vs slm 3d printing for metal manufacturing. https://www.element.com. [Online; accessed 2-March-2017].

[4] Powder bed fusion. http://www.lboro.ac.uk/. [Online; accessed March-2-2017].

[5] Senvol Database. http://senvol.com/database/.

[6] ANSYS. http://www.ansys.com/.

[7] EOS M 280. https://www.eos.info/systems_solutions/metal/systems_equipment/eosint_m280. [Online; accessed 2-March-2017].

[8] I. Abd Aziz. *Microstructure and Mechanical Properties of Ti-6Al-4V Produced by Selective Laser Sintering of Pre-alloyed Powders*. PhD thesis, The University of Waikato, 2010.

[9] M. Alarra, S. Zucca, and M. Gola. Effect of crowning of dovetail joints on turbine blade root damping. *Key Engineering Materials*, 347:312–322, 2007.

[10] American Society of Mechanical Engineering. Code of ethics. https://www.asme.org/.

[11] BeAM. http://www.beam-machines.fr/en/products. [Online; accessed 21-March-2017].

[12] B. E. Carroll, T. A. Palmer, and A. M. Beese. Anisotropic tensile behavior of ti–6al–4v components fabricated with directed energy deposition additive manufacturing. *Acta Materialia*, 87:309–320, 2015.

[13] J. Chroft. NBAA: GE techX fan blisk is all the buzz. www.flightglobal.com. [Online; accessed 2-February-2017].

[14] L. Dautova, S. Mironets, A. Klucha, and W. V. Twelves. Local contamination detection in additive manufacturing, Apr. 25 2014. US Patent App. 14/785,915.

[15] A. Designation. E466-07, standard practice for conducting force controlled constant amplitude axial fatigue tests of metallic materials. *ASTM International*, 2007.

[16] B. Dutta and F. S. Froes. The additive manufacturing (am) of titanium alloys. *Metal Powder Report*, 2017.

[17] E. e-manufacturing solutions. `https://www.eos.info/en`. [Online; accessed 13-February-2017].

[18] P. Edwards, A. O'Conner, and M. Ramulu. Electron beam additive manufacturing of titanium components: properties and performance. *Journal of Manufacturing Science and Engineering*, 135(6):061016, 2013.

[19] P. Edwards and M. Ramulu. Fatigue performance evaluation of selective laser melted Ti-6Al-4V. *Materials Science and Engineering: A*, 598:327–337, 2014.

[20] K. Ek. Additivt tillverkat material, 2014.

[21] A. M. M. García. *BLISK fabrication by linear friction welding*. INTECH Open Access Publisher, 2011.

[22] I. Gibson, D. W. Rosen, B. Stucker, et al. *Additive manufacturing technologies*, volume 238. Springer, 2010.

[23] H. Gong, K. Rafi, H. Gu, T. Starr, and B. Stucker. Analysis of defect generation in Ti-6Al-4V parts made using powder bed fusion additive manufacturing processes. *Additive Manufacturing*, 1:87–98, 2014.

[24] D. Greitemeier, F. Palm, F. Syassen, and T. Melz. Fatigue performance of additive manufactured tial6v4 using electron and laser beam melting. *International Journal of Fatigue*, 94:211–217, 2017.

[25] D. Harris. Jet engine, *How Products are Made*. `www.madehow.com/Volume-1/Jet-Engine.html`. [Online; accessed 2-February-2017].

[26] A. Hershcovitch. High-pressure arcs as vacuum-atmosphere interface and plasma lens for nonvacuum electron beam welding machines, electron beam melting, and nonvacuum ion material modification. *Journal of Applied Physics*, 78(9):5283–5288, 1995.

[27] T. W. K. N. Hiroshi Kuroki, Koji Nezaki. Application of linear friction welding technique to aircraft engine parts. *IHI Engineering Review*, 47(1):40–43, 2014.

[28] M. Khaing, J. Fuh, and L. Lu. Direct metal laser sintering for rapid tooling: processing and characterisation of eos parts. *Journal of Materials Processing Technology*, 113(1):269–272, 2001.

[29] W. King, A. Anderson, R. Ferencz, N. Hodge, C. Kamath, S. Khairallah, and A. Rubenchik. Laser powder bed fusion additive manufacturing of metals; physics, computational, and materials challenges. *Applied Physics Reviews*, 2(4):041304, 2015.

[30] P. Kobryn and S. Semiatin. Mechanical properties of laser-deposited ti-6al-4v. In *Solid Freeform Fabrication Proceedings*, pages 6–8. Austin, 2001.

[31] A. Leicht and E. O. Wennberg. *Analyzing the Mechanical Behavior of Additive Manufactured Ti-6Al-4V Using Digital Image Correlation.* PhD thesis, Chalmers University of Technology, 2015.

[32] S. Leuders, M. Thöne, A. Riemer, T. Niendorf, T. Tröster, H. Richard, and H. Maier. On the mechanical behaviour of titanium alloy tial6v4 manufactured by selective laser melting: Fatigue resistance and crack growth performance. *International Journal of Fatigue*, 48:300–307, 2013.

[33] Q. C. Liu, J. Elambasseril, S. J. Sun, M. Leary, M. Brandt, and P. K. Sharp. The effect of manufacturing defects on the fatigue behaviour of ti-6al-4v specimens fabricated using selective laser melting. In *Advanced Materials Research*, volume 891, pages 1519–1524. Trans Tech Publ, 2014.

[34] T. Material. Welding of titanium alloys. `http://www.totalmateria.com/Article28.htm`, 2001. [Online; accessed 23-Mars-2017].

[35] D. Mori. Technical data lasertec 65 3d. `http://en.dmgmori.com/products/lasertec/lasertec-additivemanufacturing/lasertec-65-3d#Technic`. [Online; accessed 21-Mars-2017].

[36] A. Nycz, A. I. Adediran, M. W. Noakes, and L. J. Love. Large scale metal additive techniques review. Technical report, Oak Ridge National Laboratory (ORNL), Oak Ridge, TN (United States). Manufacturing Demonstration Facility (MDF), 2016.

[37] OPTOMEC. Lens 850-r systems. `https://www.optomec.com/3d-printed-metals/lens-printers/metal-component-repair-3d-printer/`. [Online; accessed 21-Mars-2017].

[38] C. Qiu, G. Ravi, C. Dance, A. Ranson, S. Dilworth, and M. M. Attallah. Fabrication of large ti–6al–4v structures by direct laser deposition. *Journal of Alloys and Compounds*, 629:351–361, 2015.

[39] S. Rawal, J. Brantley, and N. Karabudak. Additive manufacturing of Ti-6Al-4V alloy components for spacecraft applications. In *Recent Advances in Space Technologies (RAST), 2013 6th International Conference on*, pages 5–11. IEEE, 2013.

[40] W. J. Sames, F. List, S. Pannala, R. R. Dehoff, and S. S. Babu. The metallurgy and processing science of metal additive manufacturing. *International Materials Reviews*, 61(5):315–360, 2016.

[41] N. Saresh, M. G. Pillai, and J. Mathew. Investigations into the effects of electron beam welding on thick ti–6al–4v titanium alloy. *Journal of Materials Processing Technology*, 192:83–88, 2007.

[42] Sciaky Inc. `http://www.sciaky.com/`. [Online; accessed 13-February-2017].

[43] Sciaky Inc. Metal additive manufacturing systems. the ebam™ 300 system. http://www.sciaky.com/additive-manufacturing/metal-additive-manufacturing-systems, 2017. [Online; accessed 9-February-2017].

[44] M. Simonelli, Y. Y. Tse, and C. Tuck. The formation of $\alpha+\ \beta$ microstructure in as-fabricated selective laser melting of Ti-6Al-4V. *Journal of Materials Research*, 29(17):2028–2035, 2014.

[45] A. Standard. E111. *Standard test method for Young's modulus, tangent modulus and chord modulus, American Society of Testing and Materials Standards*, 1997.

[46] A. Standard. E8," standard test methods for tension testing of metallic materials. *Annual book of ASTM standards*, 3:57–72, 2004.

[47] A. J. Sterling, B. Torries, N. Shamsaei, S. M. Thompson, and D. W. Seely. Fatigue behavior and failure mechanisms of direct laser deposited ti–6al–4v. *Materials Science and Engineering: A*, 655:100–112, 2016.

[48] A. B. Sundström, Bengt. *Handbok och formelsamling i hållfasthetslära*. Institutionen för hållfasthetslära, Tekniska högsk., 2014.
Note: Source is in Swedish.

[49] AZO materials. Titanium alloys - ti6al4v grade 5. http://www.azom.com/properties.aspx?ArticleID=1547. [Online; accessed 7-March-2017].

[50] EOS e-manufacturing solutions. EOS M 290. https://www.eos.info/eos-m290. [Online; accessed 9-February-2017].

[51] B. Vrancken, L. Thijs, J.-P. Kruth, and J. Van Humbeeck. Heat treatment of ti6al4v produced by selective laser melting: Microstructure and mechanical properties. *Journal of Alloys and Compounds*, 541:177–185, 2012.

[52] D. I. Wimpenny, P. M. Pandey, and L. J. Kumar. *Advances in 3D Printing & Additive Manufacturing Technologies*. Springer, 2016.

[53] X. Wu, J. Liang, J. Mei, C. Mitchell, P. Goodwin, and W. Voice. Microstructures of laser-deposited ti–6al–4v. *Materials & design*, 25(2):137–144, 2004.

[54] M. I. Yassin Mustafa Ahmed, Khairul Salleh Mohamed Sahari. Welding of titanium (ti-6al-4v) alloys: A review. 2012.

[55] O. Younossi, M. V. Arena, R. M. Moore, M. Lorell, and J. Mason. Military jet engine acquisition: Technology basics and cost-estimating methodology. Technical report, DTIC Document, 2002.

[56] Q. ZENG, Z. XUa, Y. TIAN, and Y. QINa. Progress of the modelling of a direct energy deposition process in additive manufacturing.

[57] X. Zhang, F. Martina, J. Ding, X. Wang, and S. W. Williams. Fracture toughness and fatigue crack growth rate properties in wire+ arc additive manufactured ti-6al-4v. *Fatigue & Fracture of Engineering Materials & Structures*, 2016.

[58] X. Zhao, S. Li, M. Zhang, Y. Liu, T. B. Sercombe, S. Wang, Y. Hao, R. Yang, and L. E. Murr. Comparison of the microstructures and mechanical properties of ti–6al–4v fabricated by selective laser melting and electron beam melting. *Materials & Design*, 95:21–31, 2016.

A

Budget

Item	Unit	Quantity	Vendor	Unit Price	Total Price
Poster	EA	1	Engineering Units	$62.24	$62.24
3D Prototype - Chalmers	EA	1	Prototyplabbet	$0.00	$0.00*
3D Prototype - PSU	EA	1	Shapeways.com	$128.32	$128.32
Travel Expenses to GKN	EA	6	Västtrafik	$11.67	$70.00
Total					$260.56

*Free access to workshop and 3D plastic prints

B

Risk Plan Table

Risk	Level	Action to Minimize	Fall Back Strategy
Project goals are too time consuming	High	Create a detailed and well thought out Gantt Chart	Discuss with supervisor and Sponsor
The main goal of the project is incorrectly interpreted	Medium	Thorough discussion with Sponsor	Discuss with supervisor and Sponsor
Loss of data	Medium	Use cloud based file management system that regularly creates back ups	Contact cloud service provider
Incorrect distribution of resources	Medium	Regularly updates to other members and an open dialog about needing help	Notify supervisor and Sponsor
Group members get sick	Medium	General hygiene	Inform absent student of missed work
Group members get very sick	Medium	Take care of eachother	Notify supervisor and find a solution
Incorrect information results in unnecessary work being done	Low	Ask specific questions, make no assumptions, be critical of information	Work more thoroughly with actions to minimize
Monetary resources are inadequate	Low	Plan expenses	Further limit project scope or request additional funding
Poor communication results in double work	Low	Rigorous diary writing. Start each work session with reviewing what work have been done by others	Review diary and communication processes
Change to daylight saving dates do not match, resulting in missed meetings	Low	Check ahead dates when daylight saving will occur in both countries	Book another meeting and make sure schedules match
3D printers break	Low	Be careful with the printers, make sure we understand them	Use another printer/-fix it
Group members need to learn software they are unfamiliar with	Low	Use software that have been used in previous courses	Contact someone with knowledge of the software

C

Patents

C.1 Patent US2009283503

A method for manufacturing integrally bladed rotors by laser brazing a rotor disk (1) made of a nickel or titanium-base material to blades (3) made of titanium aluminide. A brazing metal similar to the blade material is used, which is introduced into the laser beam (4) as brazing power jet (5) and whose heat capacity, which is controlled by the melting temperature and the volume of the molten metal bath This provides for melting of the disk material and alloying with this material, but not for melting of the blade material, to which it is connected by adhesion. Such blisk features a low blade weight, reduced centrifugal effects and enhanced service life.

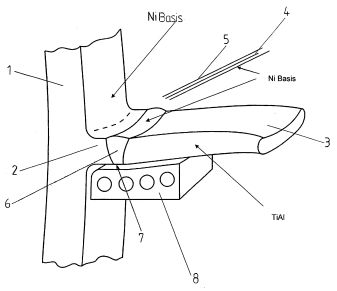

C.2 Patent US2016348517

A method of manufacturing an internally cooled blisk by additive manufacturing processes to provide weight reduction and power-to-weight ratio improvement, leading to improved efficiency, a decrease in fuel burn and lifecycle costs in an engine employing the internally cooled blisk. The method of manufacturing including defining a configuration for the internally cooled blisk, the configuration comprising a disk, an annular array of angularly spaced blades extending about a periphery of the disk and one or more internal cooling features defined within the internally cooled blisk. The method further including the step of programming the configuration into an additive manufacturing system. A powder is deposited into a chamber and an energy source is applied to the deposited powder to consolidate the powder into a cross-sectional shape corresponding to the defined configuration. Additionally provided is an internally cooled blisk.

D

Gantt Chart

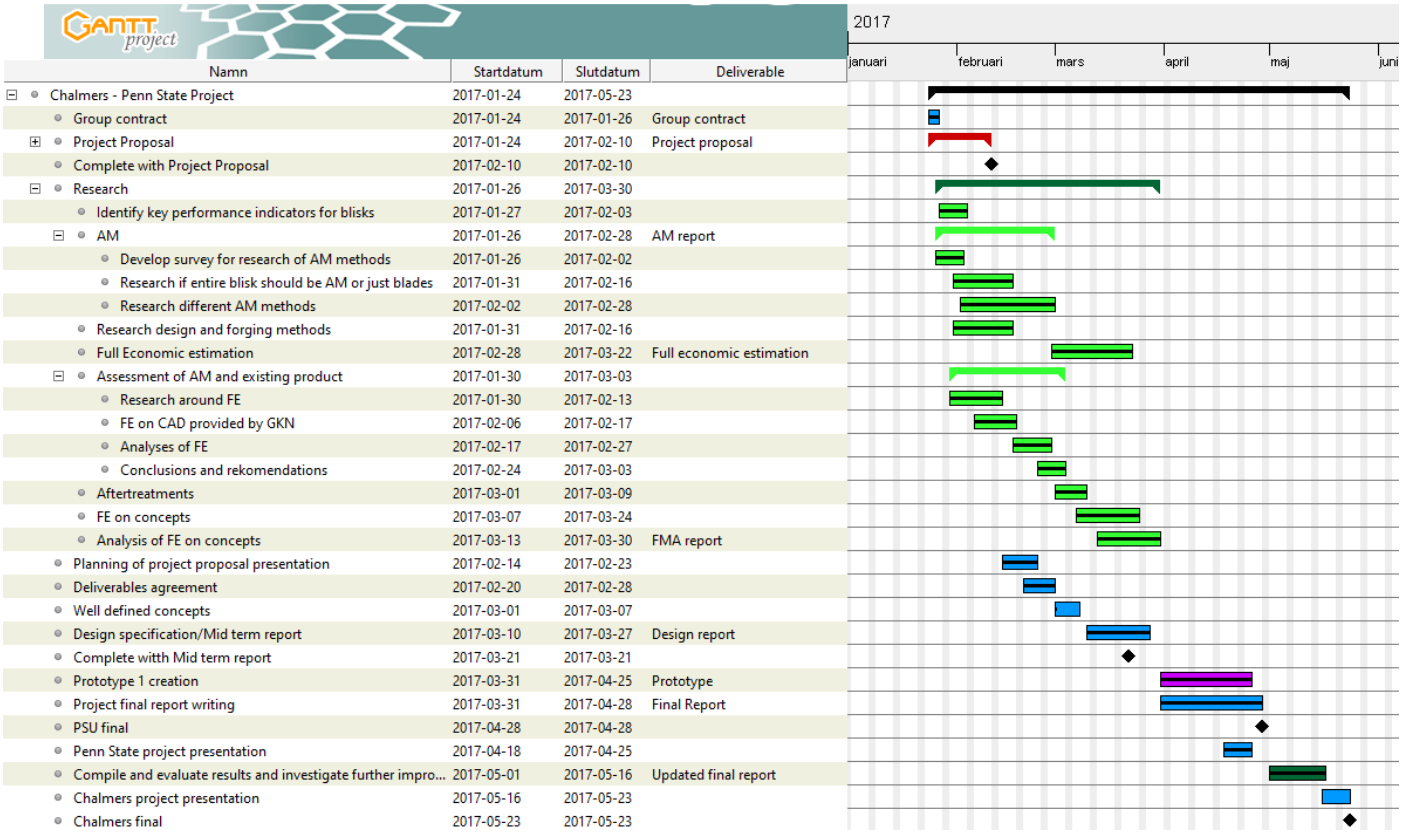

Namn	Startdatum	Slutdatum	Deliverable
Chalmers - Penn State Project	2017-01-24	2017-05-23	
Group contract	2017-01-24	2017-01-26	Group contract
Project Proposal	2017-01-24	2017-02-10	Project proposal
Complete with Project Proposal	2017-02-10	2017-02-10	
Research	2017-01-26	2017-03-30	
Identify key performance indicators for blisks	2017-01-27	2017-02-03	
AM	2017-01-26	2017-02-28	AM report
Develop survey for research of AM methods	2017-01-26	2017-02-02	
Research if entire blisk should be AM or just blades	2017-01-31	2017-02-16	
Research different AM methods	2017-02-02	2017-02-28	
Research design and forging methods	2017-01-31	2017-02-16	
Full Economic estimation	2017-02-28	2017-03-22	Full economic estimation
Assessment of AM and existing product	2017-01-30	2017-03-03	
Research around FE	2017-01-30	2017-02-13	
FE on CAD provided by GKN	2017-02-06	2017-02-17	
Analyses of FE	2017-02-17	2017-02-27	
Conclusions and rekomendations	2017-02-24	2017-03-03	
Aftertreatments	2017-03-01	2017-03-09	
FE on concepts	2017-03-07	2017-03-24	
Analysis of FE on concepts	2017-03-13	2017-03-30	FMA report
Planning of project proposal presentation	2017-02-14	2017-02-23	
Deliverables agreement	2017-02-20	2017-02-28	
Well defined concepts	2017-03-01	2017-03-07	
Design specification/Mid term report	2017-03-10	2017-03-27	Design report
Complete witth Mid term report	2017-03-21	2017-03-21	
Prototype 1 creation	2017-03-31	2017-04-25	Prototype
Project final report writing	2017-03-31	2017-04-28	Final Report
PSU final	2017-04-28	2017-04-28	
Penn State project presentation	2017-04-18	2017-04-25	
Compile and evaluate results and investigate further impro...	2017-05-01	2017-05-16	Updated final report
Chalmers project presentation	2017-05-16	2017-05-23	
Chalmers final	2017-05-23	2017-05-23	

E

Mechanical Joining Processes

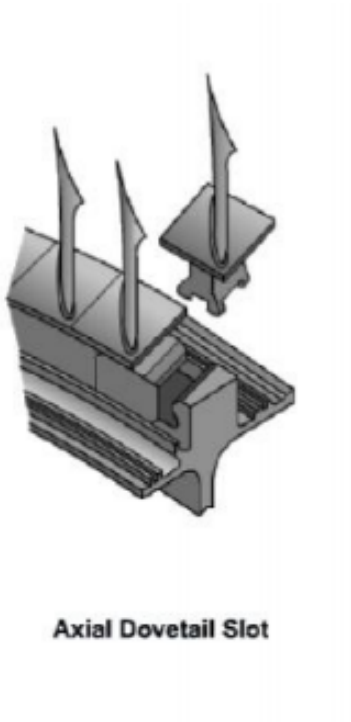

Figure E.1: Each blade is fitted using an axial dovetail slot

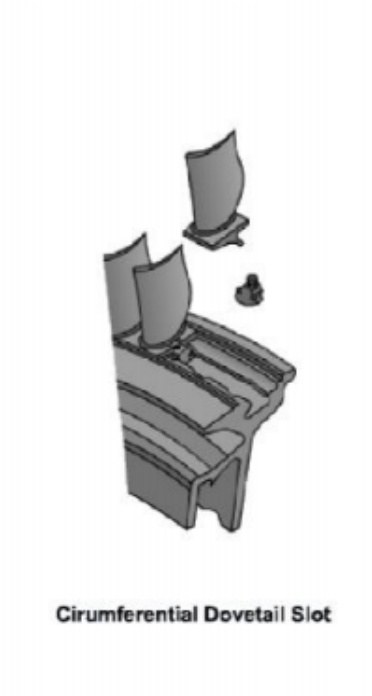

Figure E.2: Blades are fitted in a slot on the outer rim of the disk

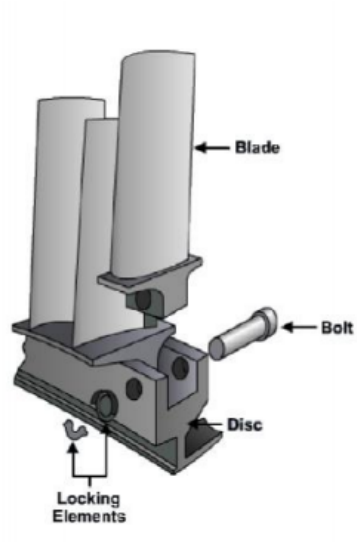

Figure E.3: A locking pin holds the blade in place

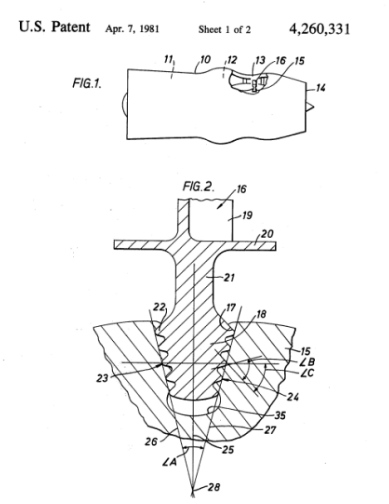

Figure E.4: A dovetail like contraption but with a fir tree shaped profile, Patent US 4260331 A

F

Campbell Diagrams

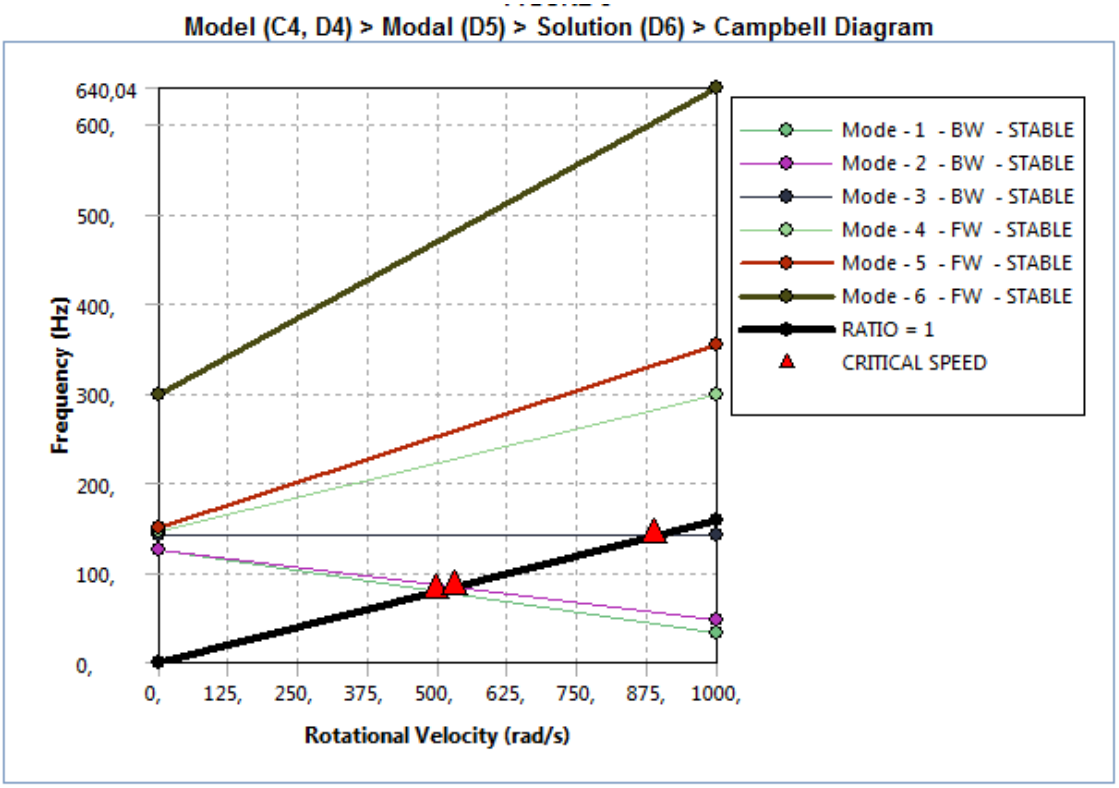

Figure F.1: Campbell diagram with pressures on the blades with machined EBM, see Table 3.5

Table F.1: Campbell table with pressures on the blades with machined EBM, see Table 3.5

Mode	Whirl Dir.	Mode Stab.	Crit. Speed	0, rad/s	1000, rad/s
1	BW	Stable	497,92 rad/s	125,28 Hz	32,826 Hz
2	BW	Stable	529,03 rad/s	126,02 Hz	46,961 Hz
3	BW	Stable	886,51 rad/s	141,94 Hz	140,98 Hz
4	FW	Stable	0 rad/s	146,01 Hz	298,97 Hz
5	FW	Stable	0 rad/s	150,25 Hz	353,5 Hz
6	FW	Stable	0 rad/s	299,02 Hz	640,04 Hz

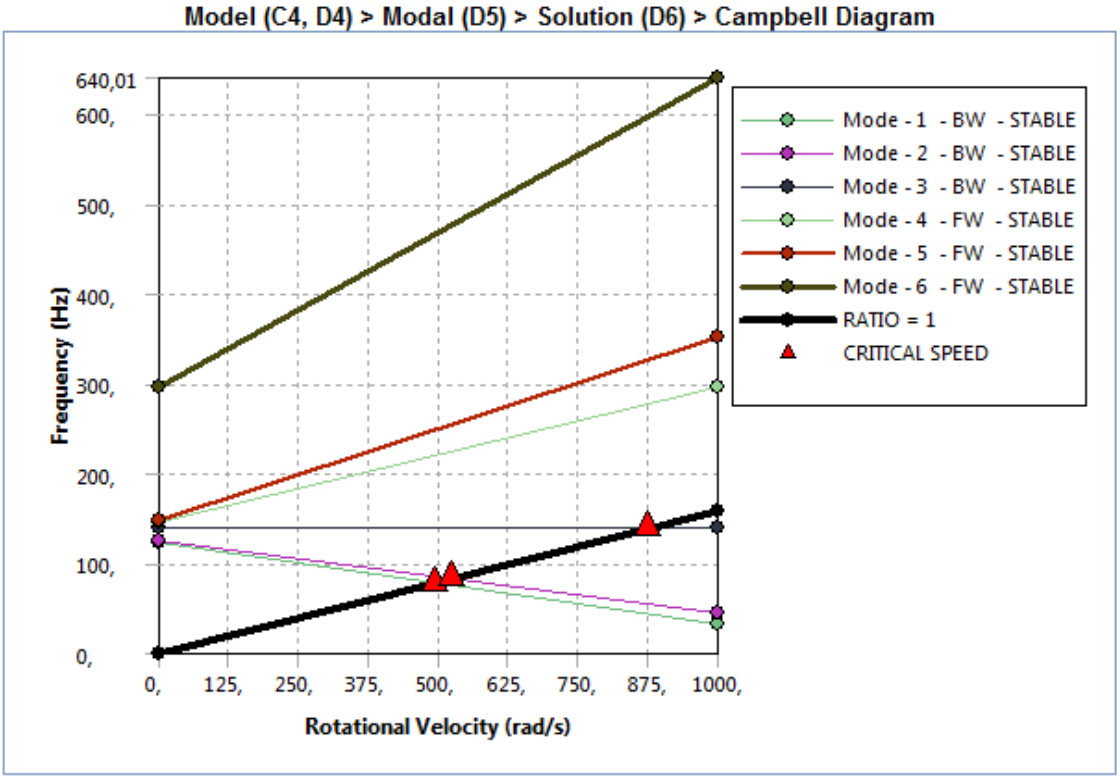

Figure F.2: Campbell diagram with pressures on the blades with machined SLM, see Table 3.6

Table F.2: Campbell table with pressures on the blades with machined SLM, see Table 3.6

Mode	Whirl Dir.	Mode Stab.	Crit. Speed	0, rad/s	1000, rad/s
1	BW	Stable	494,4 rad/s	123,86 Hz	32,49 Hz
2	BW	Stable	524,34 rad/s	124,63 Hz	46,094 Hz
3	BW	Stable	874,59 rad/s	140,08 Hz	139,07 Hz
4	FW	Stable	0 rad/s	145,65 Hz	296,01 Hz
5	FW	Stable	0 rad/s	149,2 Hz	352,57 Hz
6	FW	Stable	0 rad/s	296,03 Hz	640,01 Hz

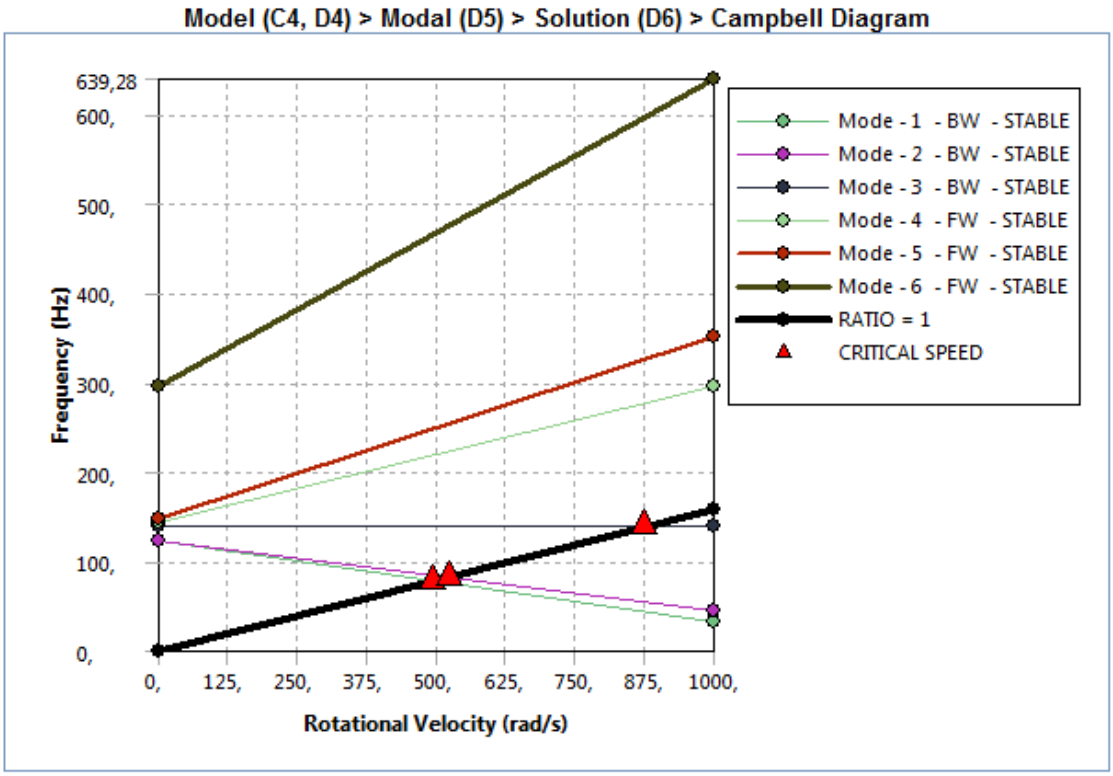

Figure F.3: Campbell diagram with pressures on the blades with machined DMLS, see Table 3.7

Table F.3: Campbell table with pressures on the blades with machined DMLS, see Table 3.7

Mode	Whirl Dir.	Mode Stab.	Crit. Speed	0, rad/s	1000, rad/s
1	BW	Stable	492,72 rad/s	123,47 Hz	32,036 Hz
2	BW	Stable	522,71 rad/s	124,18 Hz	45,766 Hz
3	BW	Stable	873,59 rad/s	139,92 Hz	138,91 Hz
4	FW	Stable	0 rad/s	144,36 Hz	295,06 Hz
5	FW	Stable	0 rad/s	148,09 Hz	352,31 Hz
6	FW	Stable	0 rad/s	295,11 Hz	639,28 Hz

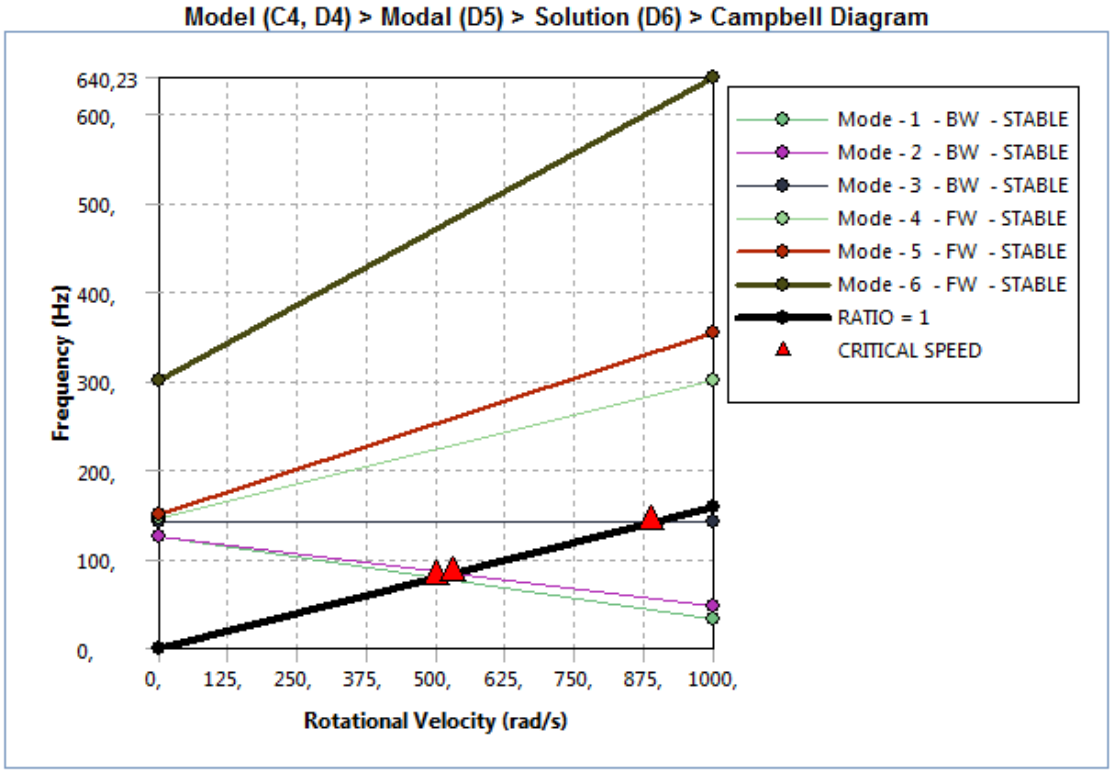

Figure F.4: Campbell diagram with pressures on the blades with machined DED, see Table 3.8

Table F.4: Campbell table with pressures on the blades with machined DED, see Table 3.8

Mode	Whirl Dir.	Mode Stab.	Crit. Speed	0, rad/s	1000, rad/s
1	BW	Stable	498,95 rad/s	125,59 Hz	33,036 Hz
2	BW	Stable	530,2 rad/s	126,34 Hz	47,21 Hz
3	BW	Stable	888,73 rad/s	142,37 Hz	141,33 Hz
4	FW	Stable	0 rad/s	146,47 Hz	299,9 Hz
5	FW	Stable	0 rad/s	150,86 Hz	353,81 Hz
6	FW	Stable	0 rad/s	300,0 Hz	640,23 Hz